METHODS AND PROCEDURES FOR LOCALIZED IN VIVO ^{31}P MAGNETIC RESONANCE SPECTROSCOPY--A NEW MODALITY OF DIAGNOSTIC RADIOLOGY

By

WEI-PENG KUAN

A DISSERTATION PRESENTED TO THE GRADUATE SCHOOL
OF THE UNIVERSITY OF FLORIDA
IN PARTIAL FULFILLMENT OF THE REQUIREMENTS
FOR THE DEGREE OF DOCTOR OF PHILOSOPHY

UNIVERSITY OF FLORIDA

1989

ACKNOWLEDGMENTS

To Dr. K. N. Scott, I wish to express my most sincere gratitude and deepest appreciation not only for introducing me to this wonderful research field, In Vivo Nuclear Magnetic Resonance Spectroscopy and Imaging, but also for her constant support and individual attention. Her friendly attitude and intelligent guidance have been a source of inspiration and encouragement. My graduate education could not have been made possible without her.

Invaluable aid and advice received from Dr. J. R. Fitzsimmons for RF coil design and construction, as well as understanding of NMR hardware, had helped tremendously during the research period. His assistance is gratefully acknowledged.

My special thanks go to Dr. T. H. Mareci for his constant suggestions in my learning of NMR physics.

To Dr. E. R. Andrew and Dr. G. S. Roessler, I wish to express my gratitude for giving their busy and valuable time to the reading of this dissertation.

I particularly thank my wife, Lee-hui, for her spiritual support and patience during my graduate education.

TABLE OF CONTENTS

		Page
ACKNOWLEDGMENTS		ii
LIST OF TABLES		v
LIST OF FIGURES		vi
ABSTRACT		viii
CHAPTER		
I	INTRODUCTION	1
II	ABSOLUTE METABOLITE CONCENTRATIONS MEASURED BY NMR SPECTROSCOPY	8
	The Importance of Absolute Quantitation	8
	Difficulties and Requirements	9
	Method for Superficially Located Sample	13
	Method for Deep-Seated Sample	22
III	PRACTICAL ASPECTS OF LOCALIZATION TECHNIQUES	28
	The Essence of Localization	28
	ISIS Localization	33
	Surface Coil Localization	45
	Relaxation Effects in Accuracy of Localization	47
	Localized Shimming	50
	Fractional Tissue Components	55
IV	RF COIL FOR IN VIVO NMR SPECTROSCOPY	60
	The Importance of and Requirements for RF Coils	60
	Coil Design Theory	63
	Method of Comparison	66
	Results and Discussion	70

V IN VIVO ^{31}P MRS OF MOUSE-TUMOR AND CAT-BRAIN HYPOXIA 74

In Vivo ^{31}P MRS of Human Osteosarcoma in Nude Mice..... 74
In Vivo ^{31}P MRS of Cat-Brain Hypoxia..... 84

VI SIGNIFICANCE AND CONCLUSIONS..... 111

APPENDICES

A DUAL-GAUGE TECHNIQUE FOR COMPUTER TOMOGRAPHY..... 116

B QUANTITATION METHOD FOR ABSOLUTE MOLAR CONCENTRATIONS..... 119

REFERENCES..... 121

BIOGRAPHICAL SKETCH..... 124

LIST OF TABLES

TABLE		PAGE
1	PCr and β-NTP NMR visible concentrations of normal mouse gluteus muscle from in vivo ^{31}P MRS	20
2	Characteristics of B_0-gradient localization methods	30
3	Characteristics of B_1-gradient localization methods	32
4	Coil performance comparison of three double-tuned coils with single-tuned coil	71
5	Summary of changes of ^{31}P metabolites and pHi in cat's brain before, during, and after hypoxia for Group I cats	96
6	Summary of changes of ^{31}P metabolites and pHi in cat's brain before, during, and after hypoxia for Group II cats	102

LIST OF FIGURES

FIGURE		PAGE
1	^{1}H and ^{31}P spectra of phantom filled with NaH_2PO_4 in NaCl solution with microsphere filled with HCCTP dissolved in benzene on top.....	15
2	^{1}H and ^{31}P spectra of mouse gluteus muscle in vivo with microsphere filled with HCCTP in benzene on top.....	16
3	^{1}H and ^{31}P tip angle matching with fixed transmitter power by varying pulse widths.....	17
4	The ratio of signal intensity at ^{1}H and ^{31}P frequencies as a function of aqueous NaH_2PO_4 concentrations.....	20
5	Representative ^{1}H images and ^{31}P spectra for in vivo absolute molar concentration measurement using ISIS.....	26
6	Representative ^{1}H images and ^{31}P spectra using flat surface coil and half-saddle coil of cat brain.....	34
7	90° hard pulse and 180° hyperbolic-secant pulse calibration curve at ^{31}P frequency.....	39
8	Calibration curves at ^{1}H and ^{31}P frequencies with gradient strength vs. slice thickness for 5 ms hyperbolic-secant pulse width.....	40
9	Demonstration of spectral localization using ISIS.....	42
10	Demonstration of spectral localization using ISIS.....	43
11	T_1 effect on spatial localization using surface coil.....	49

12	B_0 homogeneity adjustment with and without localized shimming in phantom and in vivo.....	53
13	^{31}P spectra from volumes of interest by varying sizes using ISIS--A demonstration of fractional tissues effect.....	57
14	Resonance circuits of single- and double-tuned coils and associated configurations.....	64
15	Characteristic curves of Schnall's double-tuned coil.....	69
16	Typical ^{31}P spectra of subcutaneously implanted human osteosarcoma in nude mice.....	78
17	Changes in tumor volumes and ^{31}P metabolites of osteosarcoma in mouse #1 during untreated growth.....	79
18	Changes in tumor volumes and ^{31}P metabolites of osteosarcoma in mouse #2 during untreated growth.....	80
19	Changes in tumor volumes and ^{31}P metabolites of osteosarcoma in mouse #3 during untreated growth.....	81
20	Four consecutive slices of a cat's head using multi-sliced T_2-weighted spin-echo sequence.....	93
21	Typical ISIS-localized ^{31}P spectra before, during, and after hypoxia--Group I.....	94
22	Time course plot of the changes in PCr and Pi during and after hypoxia--Group I.....	97
23	Time course plot of the changes in PCr/Pi and pHi during and after hypoxia--Group I.....	98
24	Time course plot of the changes in β-NTP during and after hypoxia--Group I.....	99
25	Typical ISIS-localized ^{31}P spectra before, during, and after hypoxia--Group II.....	101
26	Time course plot of the changes in ^{31}P and Pi during and after hypoxia--Group II.....	103

27	Time course plot of the changes in PCr/Pi and pHi during and after hypoxia--Group II.....	104
28	Time course plot of the changes in β-NTP during and after hypoxia--Group II.....	105
29	A preliminary scanning system design for CT using dual-gauge principle.....	118

Abstract of Dissertation Presented to the Graduate School of the University of Florida in Partial Fulfillment of the Requirements for the Degree of Doctor of Philosophy

METHODS AND PROCEDURES FOR LOCALIZED IN VIVO ^{31}P MAGNETIC RESONANCE SPECTROSCOPY--A NEW MODALITY OF DIAGNOSTIC RADIOLOGY

By

Wei-Peng Kuan

December 1989

Chairman: Dr. K. N. Scott
Major Department: Nuclear Engineering Sciences

Phosphorus nuclear magnetic resonance spectroscopy (^{31}P MRS) has become a novel method to study biochemistry, physiology, and metabolic process within living tissue. The noninvasive and nondestructive features of in vivo ^{31}P MRS are especially attractive and valuable for the study of human diseases. Used hand in hand with magnetic resonance imaging (MRI), in vivo MRS has stimulated a great deal of interest in the medical community. The potential use and limitation of this technique for biomedical research are examined in this dissertation.

In order to compare data from ex vivo and in vivo, and data from normal and diseased tissues, there is need for absolute metabolite molar concentration determination. For this reason, we have

developed, examined, and optimized two absolute metabolite concentration methods: one for superficial tissue and one for deep-seated tissue.

To obtain spectra from a specific region within the sample, accurate localization is needed. Factors that affect the accuracy of localization and quality of localized spectrum were examined in detail. We have reviewed existing localization methods, demonstrated the accuracy of the ISIS sequence, determined slice thickness-gradient curves, calculated the chemical shift displacement, evaluated T_1 relaxation effect, estimated effects of localized shimming and proposed a mathematical model to improve fractional tissue effect.

Three different double-tuned coils were evaluated for their characteristics and performance for optimizing signal to noise ratio and enhancing sensitivity. One, the trap-circuit design, was chosen to be used for in vivo study in this research.

Specific application to the static study of bone tumors in mice and dynamic study of hypoxia in cat brain were addressed. Changes in ^{31}P metabolite concentrations were found to be related to tumor growth in the mouse study. In the cat study, the PCr/Pi was found useful for assessment of tissue damage and for prediction of neurologic outcome after hypoxia.

CHAPTER I
INTRODUCTION

The ability to view a body structure clearly and without interference from other regions has been the goal of medical radiology ever since the discovery of X-rays by Wilhelm Roentgen in 1895. Because of clinical need, several techniques using X-rays to form images (transmission imaging) such as fluoroscopy, cinefluorography, and mammography, were developed. In 1921, focal-plane tomography was first introduced into X-ray transmission imaging. Focal-plane tomography blurs out the shadows of superimposed structures in order to show more clearly the principal structures examined. However, the main disadvantage of focused tomography is the presence of unwanted planes. About fifty years later in 1972, Hounsfield [1] introduced an X-ray computer tomography (CT) scanner, by which the distribution of linear attenuation coefficients within a layer may be determined. This technique had an explosive impact in diagnostic radiology. The outstanding sensitivity provided by X-ray CT has made possible the differentiation of much narrower density differences than has ever been possible before. For instance, it is not only possible to distinguish the cerebral spinal fluid from brain tissue, but the fine distinction between white and gray matter is also discernible.

The ability to do histological analysis in vivo has long been a dream for the clinicians. X-ray attenuation at moderate energy involves two contributions: Compton scattering effect, which is proportional to electron density and dominates at higher energy (200 kev - 2 Mev), and photoelectric absorption effect, which depends on atomic number (~ Z^{4-5}) and dominates at low energy (0-200 kev). One approach toward the goal of separating these two variables and displaying them individually in images has been proposed by Kuan and Mauderli [2]. This "Dual-gauge" technique is based on the fact that "the response of two radiation gauges have different relative sensitivities to different types of interactions between radiation and matter (mainly Compton scattering and photoelectric absorption)." This dual-gauge technique enables us to obtain density, effective atomic number and linear attenuation coefficient separately. These spatial distributions in an image have the potential of being used as better markers of various tissues, thus enabling the evaluation of the tissues' physiological and pathological character. (A more detailed description of this technique is given in Appendix A.)

X-ray techniques make use of transmitted radiation and are called transmission imaging. In contrast, nuclear medicine makes use of the emitted radiation from the radioactive nuclides injected into the body and is therefore called emission imaging. The first emission imaging technique used a rectilinear scanner. Such a scanner uses a single radiation gauge and scans back and forth over the area of interest on the patient to form an image. Later, using

multiple gauges, the Anger camera was invented which allowed dynamic, rapid-sequence imaging studies, because of a much shorter acquisition time. By adopting similar reconstruction algorithms as used in the CT scanner, the Anger camera was used to form an image of a body section representing the concentration distribution of the radioisotope used. This technique, SPECT (single photon emission computer tomography), together with PET (positron emission tomography) which uses positron-emission radioisotopes as a radioactive source, will greatly improve diagnostic radiology capability by not only studying the body structures but also body function. However, the quality of nuclear medicine images is limited by several factors: (1) Spatial resolution, which is limited by collimator resolution since the collimator hole diameter must be relatively large to provide reasonable radiation detection efficiencies. This results in blurring of the image by an amount at least as great as the hole diameters. Spatial resolution is also limited by intrinsic resolution which is due to statistical variations in the distribution of photons among the radiation detectors. (2) Contrast, which is affected by the choice of radiopharmaceutical which will give the maximum lesion-to-background uptake concentration ratio. Contrast is also affected by other instrumental and physical factors, such as film contrast and background activity. (3) Noise, which includes both random noise, which refers to random statistical variation in counting rate and structural noise which refers to nonrandom variation in counting rate superimposition and machine noise. Nuclear medicine due to

its rather poor resolution has limited applications, despite the fact that it gives a lot of functional information.

Ultrasound is capable of providing information concerning body structure and permits real-time motion studies without using ionizing radiation. However, even the latest pulsed ultrasound imaging techniques cannot provide enough spatial resolution for detailed examination. In addition, the signal intensity is a function of many variables, such as pressure, density, temperature, stiffness, and particle motion which make the interpretation of the image complex.

Nuclear magnetic resonance imaging (MRI), the newest diagnostic imaging modality, has stimulated the medical community more than any other technique since the introduction of X-ray computer tomography. One major factor for this is the capability of MRI to generate, without ionizing radiation, high resolution, diagnostic quality medical images at any angle and projection of the human body. NMR is based not only on subatomic physical principles as nuclear medicine, but also on atomic interactions. Therefore, NMR can revolutionize medical diagnostic imaging by providing, with no risk, in vivo data of human biochemistry and pathophysiology.

In recent years, nuclear magnetic resonance spectroscopy (MRS) has become a novel method to study metabolic processes in a wide variety of living beings, ranging from bacteria to humans. As in MRI, a most attractive feature of MRS is that it is noninvasive and nondestructive, since it does not use ionizing radiation such as X-

rays or radioisotopes. Early work on MRS had focused on using proton (^{1}H) spectroscopy to elucidate molecular structure; later technology was developed to permit analysis of other NMR-sensitive nuclides, most notably carbon (^{13}C). More recently, the value of studying nuclides other than ^{1}H and ^{13}C has been recognized: Some of the nuclides of interest are phosphorus (^{31}P), lithium (^{7}L), and chlorine (^{35}Cl). Among these nuclides, ^{31}P has gotten more attention than any other nuclide because the synthesis of high energy phosphates, ATP (adenosine triphosphate) and PCr (creatine phosphate), play a very important role in body physiology. These phosphate metabolite concentrations can be correlated to tissue-energy state and the health or disease condition of the tissue.

Although ^{31}P MRS has been used to study many pathological conditions, such as ischemia, glycosemia, and most commonly skeletal muscle diseases (or functions), many questions have to be answered before we can obtain good quality spectra and use them for biomedical research and, eventually, for clinical diagnostic purposes. Some of the main problems to be evaluated are the following: (1) Absolute metabolite molar concentrations measurement, not only to establish a better comparison and correlation between data from biochemical methods and those from MRS, but also to use them in comparisons of normal and metabolically disturbed states of an experimental animal or in the diagnosis of disease in human patients. Fractional changes (changes in ratio of two metabolites) in the resonance signal

intensities fail, in many cases, to be good markers of disease conditions. (2) Localization for accurate assignment of the acquired spectrum to a specific region within the whole object. (3) RF coil characteristics and performance evaluation for optimizing signal-to-noise ratio (S/N) ratio and enhancing sensitivity with emphasis on spectroscopy. Other essentials to ^{31}P MRS study are the following: Understanding of the chemical shift displacement when slice selection is used in the presence of chemically shifted species, the relaxation effects in spatial localization, the availability and accuracy of measuring intracellular pH using ^{31}P MRS, the necessity of localized localization under the effect of fractional tissue components, the experimental procedure to take full use of machine capability and to save time, and data processing. It is the purpose of the present study to understand, from both a physics and practical point of view, the effects and limitation of these factors to ^{31}P MRS. Specific applications to be addressed will be human osteosarcoma implanted into nude mice and hypoxia of the cat's brain. If we accomplish our goals, this would have the following significance: (1) If we can obtain localized spectra with improved S/N and speed, and if we can quantitate our metabolite concentrations more accurately and reliably, this would make our in vivo spectroscopy research easier and also much more meaningful.

(2) The biological results of the tumor study will aid our understanding of tumor growth and to what extent in vivo spectroscopy can follow tumor growth.

(3) If the in vivo spectroscopy results can be correlated with neurological changes following brain hypoxia in cats, this would be very helpful for patient management. If spectral changes could be correlated with reversible or irreversible neurological damage, this would be very meaningful.

(4) If we can obtain and perfect a good volume localization method for our biological models, this would be very useful. It would not only help our current studies but could be extrapolated to future studies and possibly the study of other biomedical problems.

CHAPTER II
ABSOLUTE METABOLITE CONCENTRATIONS MEASURED BY NMR SPECTROSCOPY

The Importance of Absolute Quantitation

Although ^{31}P nuclear magnetic resonance spectroscopy (MRS) has found a wide range of applications in biological and medical problems, one of the limitations to such studies has been the difficulty in quantitating the results to obtain absolute metabolite concentrations. The emphasis of these studies has been on fractional changes in the resonance signal intensities of a metabolite relative to another signal intensity in a high resolution spectrum. These relative quantitative measurements are done by taking spectra and measuring ratios of peak areas. Which ratios are chosen are based on several considerations: (1) interest in measuring "energy status," e.g., PCr/Pi (creatine phosphate/ inorganic phosphate), (2) one of the metabolites is assumed to remain constant throughout the experiment and can be used to assess changes in other metabolites of interest, e.g., PCr/NTP (nucleoside tri-phosphate), Pi/NTP, or (3) the metabolites of interest can be compared to the sum of all the metabolites in the spectrum, assuming the total amount of all metabolites remain

unchanged throughout the experiment. Because of the difficulties mentioned below, absolute metabolite concentrations have not been done in spite of their potential importance in comparisons of normal and pathological tissues of an experimental animal or in diagnosis of diseases in human patients. Evidence from biochemical examination has shown [3], for instance, that absolute phosphate metabolite levels are reduced in muscular dystrophy, chronic cerebral infarction, atrophy, and possibly dementias, despite relatively unperturbed metabolite ratios. In addition, the absolute molar concentrations are needed to calculate biomechanical reactions. This will lead to the understanding of concentration of reactants, reaction rates, and even their dynamic driving forces. This suggests that absolute metabolite concentration measurements are not only of scientific interest but may have clinical value. Clinical NMR studies made by scientists and clinicians [3] in order to measure metabolite levels have shown a growing need to obtain absolute quantitation of these metabolites to evaluate varius pathological conditions. Therefore, methods which provide accurate absolute molar concentration measurements are urgently needed for both biochemical and clinical studies.

Difficulties and Requirements

The major difficulties of derivation of absolute and some relative concentration have been (1) Accuracy of localization or

spatial resolution. This includes imperfections in slice selection, chemical shift displacement effect on slice selection, relaxation effect on sensitive volume and tissue heterogeneity. (See Chapter III for details.) (2) Nonuniformity B_1 field. Since the NMR signal intensity is proportional to the product of B_1 intensity and tip angle (which is also proportional to B_1), its variation over the sample volume may be large even within a homogeneous sample. This is more severe when a single-coil system (transceiver) is used. (See Chapter IV for details.) (3) Partial saturation of metabolites and incorrect pulse adjustment. (4) Tissue state. Metabolites (e.g., PCr) will be decreased in tissue extract, or even lost, during extraction. Conversely, other metabolites (e.g., PDE) which are bound in the cells in in vivo state may become free, and hence their concentrations increased. T_1's and T_2's may also be changed in the extract due to different ionic environments. (5) NMR visibility. Detectable NMR signals arises from metabolites provided that they are present in sufficient concentration and are sufficiently mobile. The apparent absence of metabolite in an NMR spectrum only sets an upper limit on its concentration and cannot be interpreted as that the metabolite is not present. Therefore, it is possible that concentrations derived from NMR data are well below the actual levels in vivo. For instance, phospholipids, when incorporated in membranes, do not give narrow lines; however, if the membrane is broken down for some reason, then more phosphodiesters and phosphomonoester will become NMR visible. (6) Origin of the NMR signals. Although we are interested in the intracellular

concentration, an NMR signal is an average, over the selected volume, of all the tissue types and for a given tissue type, an average of all cell types. Due to this tissue heterogeneity, one must ascertain whether a change in signal can be ascribed to the cells of interest and, if so, whether it is due to the change of intracellular volume or to intracellular metabolite concentrations since the NMR signals is proportional to the product of volume and concentration. (7) Coil loading. Biological tissues are electrically conductive and change the coil loading. This is observed in the change of coil Q when the coil is loaded. The transmitter coil will produce a different, usually smaller, B_1. The tip angle, however, can be recovered by either using higher transmitter power and/or longer pulse width. Unfortunately, the receiver coil still suffers a reduced sensitivity after loading and cannot be compensated. The importance of these effects is that any calibration procedure using a concentration standard to measure metabolite concentrations may be invalid if the standard is placed in a different position from where the biological sample is or if the coil loading effect is different between the standard and the sample. However, a method which uses a standard and is distinguishable in the same spectrum taken from the tissue of the sample will not suffer from a difference in coil loading.

Accurate measurement requires data collection and analysis to be set up properly to preserve the proportionality between peak area and concentration. In data collection (1) the repetition time should be chosen to be five times the longest T_1 of the peaks to be

measured; alternatively, a saturation factor may be measured for each peak and the partially saturated spectra used; (2) acquisition time should be chosen long enough (~ $5T_2^*$) to collect all of the free induction decay; (3) pulse width should be set short enough to cover the range of chemical shifts present in the spectrum; (4) audio frequency filter bandwidth should be set to uniform sensitivity throughout the whole frequency range; (5) amplifier gain should be examined to ensure constant spectrometer gain during the experiment. In data analysis, the parameters used to process the free induction decay must be kept constant throughout the whole process.

Several quantitative methods have been proposed. However, all present problems: (1) the coil sensitivity profile and volume of interest (VOI) must be known accurately [4]; (2) the ill-defined variable geometry of tissues is compared to the well-known geometry of phantoms used in calibration [5]; (3) internal marker method [6] requires not only invasive marker injection but a separate measurement of the marker concentration.

In order to meet the needs of two types of experiments, namely, signals from superficial site of the sample (type I) and signals from deep-seated site of the sample (type II), we have developed the following two methods.

Method for Superficially Located Sample

Introduction

For "type I" application, the method (method 1, Appendix B) adopts the principle previously described [7]. This method takes into account the effects of (i) tip angle changes (in the excitation mode) on both frequencies due to coil loading (inductive losses), (ii) coil sensitivity changes (in the receiving mode) due to coil loading, and (iii) time-dependent changes in the spectrometer gain.

Our method is as follows. The surface coil is double tuned to ^{31}P and ^{1}H. By making the tip angles at the coil center for the two nuclei the same, the spatial variations of sensitivity at the two frequencies are also matched. The ratio of ^{31}P to ^{1}H sensitivity is then independent of position and hence of sample geometry. This ratio is measured using a standard sample of known ^{31}P and ^{1}H concentrations. The ratio of ^{31}P to ^{1}H signals for tissue then gives the ratio of ^{31}P to ^{1}H concentrations. The water ^{1}H concentration in tissue is reasonably constant and is known from other measurements; hence the ^{31}P concentration can be found. We have assumed uniform ^{31}P and water ^{1}H concentration within the sensitive volume of the coil.

Method

Measurements were performed on a Spectroscopy Imaging Systems Co. model VIS 2T spectrometer. A 1-cm-diameter two-turn surface coil double tuned (see Chapter III for coil circuit, characteristics, and performance) to ^{31}P (34.6 MHz) and ^{1}H (85.5 MHz) was used to match the spatial sensitivities at these two frequencies. An 18 µl microsphere containing hexachloro-cyclotriphosphazene (HCCTP) and benzene (C_6H_6) was placed in the center of the surface coil. The HCCTP has a chemical shift difference of about 25 ppm downfield from both NaH_2PO_4 (in the phantom, Figure 1(b)) and PCr (in vivo, Figure 2(b)). Benzene has a chemical shift difference of about 5 ppm downfield from both phantom water (Figure 1(a)) and tissue water (Figure 2(a)). The tip angles were matched at ^{31}P (Figure 3(a) and ^{1}H (Figure 3(b)). Figure 3 shows the tip angle adjustment at the 18 µl microsphere placed at the center of a 1-cm surface coil by varying the pulse widths at fixed transmitter power. Pulse widths to achieve 90° and 180° tip angle were found to be 5 µs and 10 µs at 100 db transmitter power and 0 db receiver attenuation with 5 Hz line broadening for ^{31}P. They were 6 µs and 12 µs at 110 db transmitter power and 20 db receiver attenuation without line broadening for ^{1}H.

Calibration was done on a disk phantom (diameter = 5 cm, thickness = 3 cm) with phosphorus concentration (from NaH_2PO_4) ranging from 5 mM to 40 mM. Saline (sodium chloride in water)

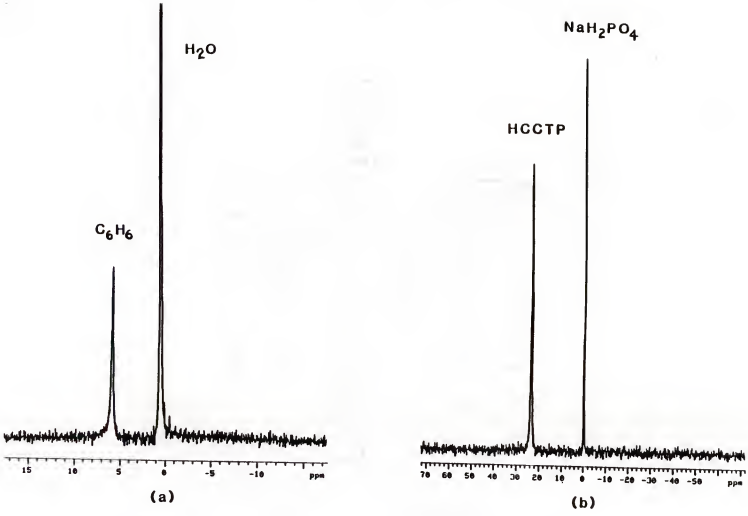

Figure 1. ^{1}H and ^{31}P spectra of a disk-shaped phantom filled with NaH_2PO_4 and NaCl dissolved in water with an 18 microliter microsphere filled with HCCTP dissolved in benzene (C_6H_6). (a) ^{1}H spectrum. (b) ^{31}P spectrum.

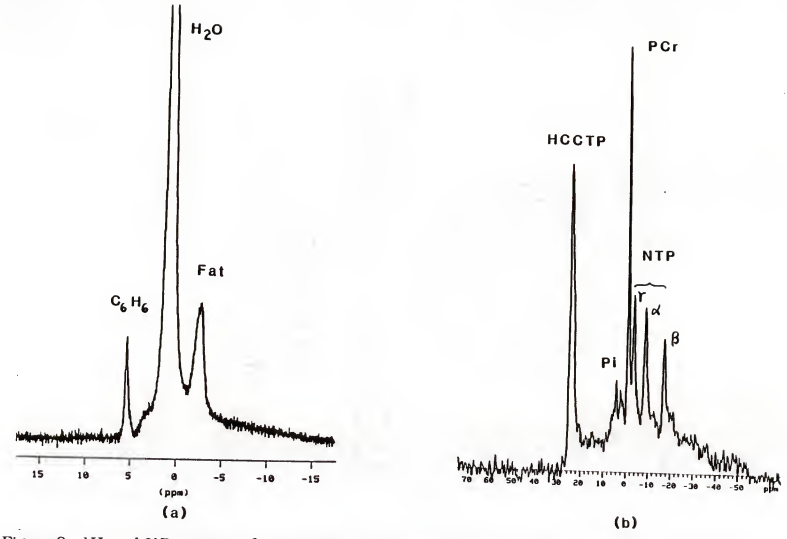

Figure 2. ^{1}H and ^{31}P spectra of mouse gluteus muscle in vivo. These spectra were obtained with a two-turn 1-cm surface coil with an 18 microliter microsphere placed in the center of the coil. (a) ^{1}H spectrum (b) ^{31}P spectrum. The water peak is partially cut for easy comparison.

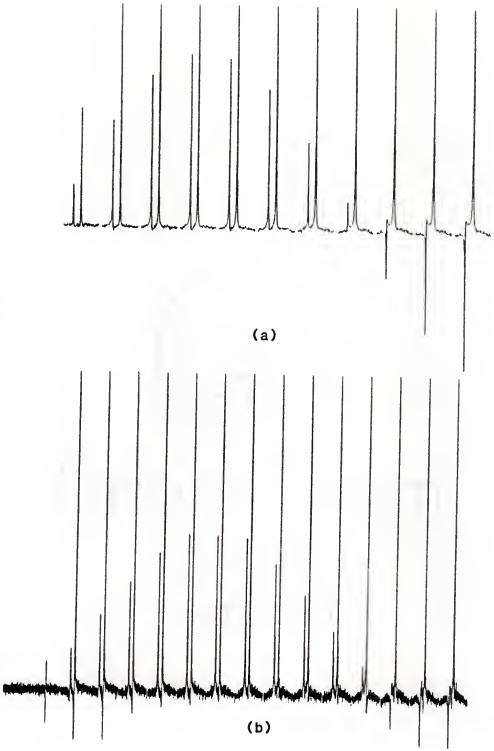

Figure 3. ^{1}H and ^{31}P tip angle matching at 18 microliter microsphere placed at the center of a 1-cm surface coil by varying pulse widths at fixed transmitter power. (a) ^{1}H calibration curve. (b) ^{31}P calibration. The peaks that show a sine wave pattern are from C_6H_6 in (a) and HCCTP in (b).

was used as solvent. The loading effect in the phantom was kept the same by adjusting the sodium chloride concentration for each ^{31}P concentration. The calibration curve, relating NaH_2PO_4 concentration to $^{31}P/^{1}H$ intensity ratio was plotted in Fig. 4. The calibration constant K, the slope of the line, was calculated by first-order linear regression method.

Results

To demonstrate the utility of this technique in vivo, we give surface coil results of concentrations of PCr and β-NTP in the gluteus muscle of nude mice. Proton and phosphorus spectra of the mice were obtained using the same surface coil with the microsphere. Tip angles were adjusted to 180° to accentuate the muscle signal and to minimize the microsphere signal and were checked, by monitoring the pulse width while the transmitter power remained fixed, at the two frequencies to make sure the loading effects were the same for the tissue as they had been for the phantom. To correct the peak intensities for partial saturation effects, T_1 values of ^{31}P in the phantom and tissue were determined using the progressive saturation pulse sequence. T_1's were found to be 2.8 sec for PCr and 1.2 sec for β-NTP. Saturation factors were calculated to be 0.66 for PCr and 0.92 β-NTP with TR = 3 sec. The tissue water concentration needed for calculating absolute metabolite concentrations was obtained by multiplying 111 M, the water concentration in the test tube, by the ratio of image

intensities of the gluteus muscle and the test tube. Data acquisition and processing parameters (sweep width, number of averages, vertical scale, line broadening, etc.) were kept constant. For tissue, the broad hump in the ^{31}P spectra due to bone and phospholipids was removed by the convolution difference method.

The calibration curve obtained from solutions of known concentrations of NaH_2PO_4 is shown in Figure 4. The calibration constant K is calculated to be 19369 by forcing the line to go through the origin. The PCr and β-NTP concentrations, given in Table 1, were obtained from five normal male nude mice, each weighing approximately 30 grams, each measured twice, a week apart. The mean muscle β-NTP concentration of 5.6 ± 0.9 mM is in good agreement with the value reported previously for the rat hind limb muscle [8] which was 6.1 mM. We found very good reproducibility of the repeat measurement for each mouse. We found fairly large variability between mice. This we attribute to differences in the individual.

Discussion

The method presented here will give quantitative results if two conditions are met: (a) The B_1 penetration is the same for both frequencies. This holds for our example, a 1-cm diameter surface coil, because the effective depths [9] are much larger than the dimension of the sensitive volume (~ 0.5 cm). However, for larger coils and deep-seated samples, the ratio of signal intensities

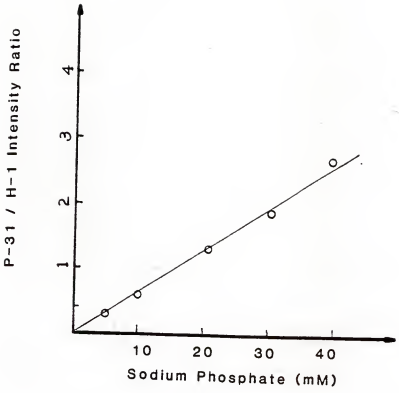

Figure 4. The ratio of signal intensities at ^{1}H and ^{31}P frequencies as a function of aqueous NaH_2PO_4 (sodium phosphate) concentrations.

TABLE 1. PCr AND β-NTP NMR VISIBLE CONCENTRATIONS OF NORMAL MOUSE GLUTEUS MUSCLE FROM IN VIVO ^{31}P MRS

Mouse	1	2	3	4	5	Mean
PCr[a]	14.5, 14.9	12.0, 13.0	10.7, 10.5	12.6, 12.8	14.1, 13.9	12.9 ±1.4
β-NTP [a]	6.6, 6.8	6.3, 7.3	5.1, 4.9	5.3, 4.7	4.8, 5.0	5.6 ±0.9

[a]Numbers separated by a comma are values from 2 measurements obtained a week apart.

recorded at two widely different frequencies may be affected by the frequency dependence of RF penetration depth (^{31}P penetration depth > ^{1}H penetration depth). (b) The metabolites must have uniform distribution within the sensitive volume, which was a good approximation for the small volume of muscle under investigation. Otherwise, tissue compartmentation effects should be taken into account.

Correction for reception efficiency differences due to the varied loading can also be done by the following method, which is based on the inverse relationship between B_1 strength and pulse width: The observed ^{31}P molar concentration is multiplied by the ratio of the pulse widths for constant microsphere tip angles with tissue and phantom loading. Due to the weak coupling of ^{1}H to tissue, we found no correction was needed in our case which indicates another advantage of this type of double-tuned coil [10]. If necessary, similar correction has to be done for ^{1}H as well as in ^{31}P for other types of coil designs which have stronger coupling.

Other than reference ^{31}P signal intensity to ^{1}H, the same method can be implemented by reference to ^{2}H (in HDO) which has a natural abundance of 17.3 mM. This has the following advantages: (1) Dynamic range problems can be avoided because ^{2}H of HDO does not require attenuation of the receiver. This results in better tip angle matching. (2) Self-resonance effect is less severe when a ^{2}H-^{31}P double-tuned coil is constructed (13 and 34.6 MHz at 2T) for use at a high field system, especially when a solenoidal coil of

high inductance is desired. (3) The ^{2}H-^{31}P coil can also be used to measure blood flow by the HDO washout method.

One of the criteria for the above method to give accurate results is that the B_1 profile of both frequencies remains the same throughout the whole sensitivity volume of the coil. This is the case when a single-pulse sequence (or other sequences without localization scheme) is used associated with a surface coil with a typical radius of about 2 cm. However, for larger coils and deep-seated volumes of interest, at high frequencies, the ratio of signal intensities recorded at two widely different frequencies (34.6 Hz and 85.5 MHz) may be affected by the frequency dependence of RF penetration depth, defined as the distance into the sample at which B_1 strength decreases to 1/e of its initial values. In this case another approach has to be used for quantitation measurement.

Method for Deep-Seated Sample

Introduction

In imaging spectrometers, several localization techniques (see Chapter III) using gradients for slice selection have been developed. For the reasons described in Chapter III, we use the ISIS localization technique [11] for absolute quantitation.

A somewhat naive method was previously proposed [12] by using a coil of "uniform" B_1 profile, such as a head coil, and therefore it was assumed that the signal integral is proportional to

volume size. The size of the selected volume was calibrated by comparing the signal from this volume to that of a small standard sample of high ^{31}P concentration using the following equation:

$$C_{met} = \frac{I_{met}}{I_{std}} \times \frac{V_{std} \times C_{std}}{V_{met}}$$

where C_{met}, C_{std} are concentration of metabolites and standard

I_{met}, I_{std} are peak intensities of metabolites, and standard.

V_{met}, V_{std} are volumes of metabolites and standard.

The difficulties in using this method are due to the following: (a) Only a small fraction of the region within the sensitive volume of a coil with uniform B_1 profile can be used, or (b) a detailed field plot of B_1 is needed and, most importantly, (c) variations in the loading of the coil caused by the sample are different between tissue and calibration standard solution. When the calibration work is done before the in vivo experiments, a compensation method of taking into account changes in coil Q and therefore sensitivity is needed.

By using ISIS, our methods are able to obtain an NMR spectrum from a VOI of well-defined shape and volume and to compare it directly with the ^{31}P spectrum from the "same" VOI relative to the coil of a standard sample, despite the nonuniformity of B_1 profile. In addition, the calibration work is done after the in vivo experiment when the loading conditions are known and can be

duplicated and matched by varying the ionic concentrations in the standard phantom. Therefore, this method is applicable to a surface coil, and no reference to the ^{1}H signal intensity is required. An external marker can be used to check the positions of the VOIs relative to the coil geometry through imaging tissue and standard phantom, and to monitor changes in tip angle and sensitivity.

Methods

Experiments were performed on a 2T Spectroscopy Imaging Systems Co. model VIS 2T spectrometer with a half-saddle coil (diameter = 8 cm, length = 8 cm) double tuned to ^{1}H and ^{31}P with the same circuit as in Method I. Localized ^{31}P MRS of the cat brain and then the phantom containing known concentration of NaH_2PO_4 within the same VOI's in positions and volumes were obtained in conjunction with ^{1}H MRI. A 2-mm-thick, multislice (usually 10 slices) spin-echo imaging sequence (TR = 500 ms, TE = 20 ms) was first used to obtain transverse and sagittal images across the sensitive region to define the center of the VOI's. B_o homogeneity was adjusted by shimming with the single-pulse sequence on the ^{1}H signal. Localized shimming with the VOSY sequence was not practical, because the size of the echo shown on the oscilloscope is too small to detect meaningful changes of echo size and shape. The ISIS sequence used to obtain localized ^{31}P MRS was modified to allow partial saturation within each of the eight ISIS experiments and complete relaxation between experiments. This is done by

using 15 sec delay time (~ 5 T_1) between experiments and 1.5 sec recovery time between scans within one experiment. This modification gives complete relaxation between experiments which minimizes contamination by signal from outside of the VOI. The hyperbolic-secant inversion pulse was used for homogeneous inversion within the coil. Spectra were processed by 300 Hz and 10 Hz line broadening and then subtraction of the two spectra. Partial saturation was avoided in the standard phantom by using a 15 sec recovery time between pulses. The T_1 was estimated to be 3 sec.

A large flask, (standard phantom, diameter = 7.5 cm, length = 10 cm) containing 5 mM NaH_2PO_4, with ~ 1 M sodium chloride to match the tissue loading condition, was placed in a double-tuned half-saddle coil and a VOI was selected within the phantom. A series of ^{31}P spectra was obtained for various volumes by varying the strengths of the selection gradients in all three directions. The data confirmed that the signal intensities were not proportional to the volume sizes (signal intensity/volume has a variation up to 30%) due to the B_1 inhomogeneity. A spectrum obtained from a VOI of 6.5 cc within the brain was obtained and then compared with the signal intensity of a spectrum from the same VOI (Fig. 5) in position and volume within the phantom obtained after the in vivo experiment. The T_1 of ^{31}P metabolites was measured by varying the time interval between the last selective pulse and the excitation pulse in the ISIS sequence. The measured T_1's of the cat brain are

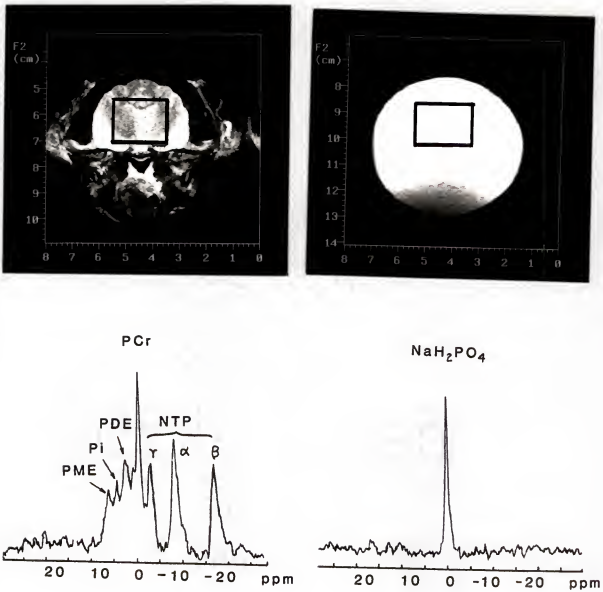

Figure 5. Representative scheme for in vivo absolute molar concentration measurement using ISIS. (a) cat head image and associated ^{31}P spectrum in brain. (b) phantom of 5 mM NaH_2PO_4 water solution and associated ^{31}P spectrum. For explanation see text.

as follows: PME, 3.5 sec; Pi, 2.6 sec; PDE, 3 sec; PCr, 3.1 sec; γ-NTP, 1.2 sec; α-NTP, 1 sec; β-NTP, 1 sec.

Results

By assuming a water concentration of 83 M (or 74.7% tissue water) within the brain, the concentrations calculated from signal intensities were PME, 4.0 mM; Pi, 4.2 mM; PDE, 6.5 mM; PCr, 7.2 mM, γ-NTP, 6.1 mM, α-NTP, 9 mM; β-NTP, 8.5 mM under normal conditions. This is, however, different from a previous study on the human brain [13], where Pi, 2.6 mM; PCr, 4.3 mM, γ-NTP, 3.5 mM, α-NTP, 5.7 mM; β-NTP, 3 mM are reported. This may be due to the difference in species. The accuracy by which concentrations can be determined is mainly limited by the accuracy of intracellular water content measurement and how well these peaks can be resolved.

In conclusion, we have developed two methods for in vivo absolute ^{31}P metabolite concentration measurement. These methods were originally designed for in vivo applications of mouse tumor and cat brain studies. However, the methods can be applied to many other in vivo ^{31}P MRS studies and MRS of other nuclides. In spite of all the efforts to perfect the quantitation methods, the difficulties of measuring the areas of overlapping peaks (especially in the Pi area which contains a hump from phospholipid in a ^{31}P spectrum) remains and will always be the major source of error, particularly in ^{31}P brain spectra.

CHAPTER III
PRACTICAL ASPECTS OF LOCALIZATION TECHNIQUES

The Essence of Localization

A major problem of in vivo MRS has been the accurate assignment of the acquired spectrum to a specific region within the sample. Undifferentiated chemical information from the whole sample, such as an animal or human, is usually of little interest. Instead, spectroscopy from a particular spot of the sample, preferably without or with little contribution from surrounding tissue, will give information about the metabolism of the area under examination. This is known as "Localized Spectroscopy." The most general experiments which yield spatial and chemical information are multidimensional methods. These, in principle, can also include T_1 and T_2 information, flow and motion information, etc. However, the tremendous time requirement and reduction in sensitivity have made such a hypothetical experiment totally nonfeasible. Therefore, many different localization methods have been suggested to acquire metabolic information from a well-delineated volume within a sample. Among these methods, many "Spectroscopic Imaging" techniques have been proposed which

yield full spectra in up to three dimensions [14] but, as expected, at considerable time expense. The most useful type of spectroscopic imaging methods, so far, which make experiments suited for in vivo application are "one-dimensional" spectroscopic imaging methods, which have selective volume in the shape of slices. However, since the sampling is performed in one spatial dimension only, in many cases, localization is not adequate. In order to further shorten acquisition time, improve sensitivity and match the shape of the sample under examination anatomically, methods have been developed by making spectroscopic imaging experiment selective in all three spatial dimensions to yield a single volume element. These are called "point methods" [15-19]. First, conventional ^1H imaging is done with good sensitivity and high speed for the visualization of the anatomy of the sample and for the proper location of the sensitive volume for spectroscopy. Then, if the localized spectroscopy is selective in all three spatial dimensions, the selective volume can be a plane, a column, or a cube, which are all termed VOI. To obtain information about the chemical composition of one or more clearly defined volumes of interest, localization methods can be classified into two main categories depending on whether B_0 of B_1 gradient is used. The common feature of the first category, "B_0-gradient" methods [15], is that they select planes in a sample by the application of frequency selective RF pulses in the presence of linear B_0 gradients. An overview of these methods and important characteristics associated with them is shown in Table 2. They can delineate volume (or volumes) from

TABLE 2. CHARACTERISTICS OF B_0-GRADIENT LOCALIZATION METHODS

Method Number	1	2	3	4	5	6
MAIN AIMS						
speed	v		v	v	v	v
sensitivity	v	v				
spectral resolution	v	v	v	v	v	v
spatial resolution	v	v	v	v	v	v
several ROIs				c	c	
one ROI	v	v	v	v	v	v
ROI near surface	v	v	v	v	v	v
ROI at depth	v	v	v	v	v	v
SHAPE OF ROI						
slice	v	v	v	v	v	v
column	v	v	v	v	v	v
cube	v	v	v	v	v	v
SAMPLE LIMITATIONS						
very low sensitivity	v	v				
very short T_2	v	v				
very wide spectra aperiodic motion	v		v	v	v	v
EQUIPMENT LIMITATIONS						
inhomogeneous B_0	v	v	v	v	v	v
weak B_1		v	v	v	v	
slow B_0 gradient	v	v				v

v:fulfills a certain criterion
c:different selected volumes must not have a common plane.

method number 1 = VSE [17]
2 = ISIS [11]
3 = SPARS [18]
4 = modified "SPARS" [19]
5 = VEST [16]
6 = SPACE [16]

which high resolution spectra can be obtained. The second category, "B_1-gradient" methods [16], makes use of B_1 gradients, usually produced by a surface coil. This type of localization method is improved by using phase cycling and/or composite pulses [20]. An overview of these methods is included in Table 3. Because of the wide variety of requirements for in vivo MRS measurement, it is unlikely that there is a universal optimum technique for all applications. The best method to use depends on many factors, such as the goal of the investigation, location and size of the VOI, animal models, and limitations inherent in the instrumentation. Tables 2 and 3 which give a summary of the advantages and disadvantages of these methods can be used as a guide in choosing which method to use. It was not the aim of this research to evaluate and compare the characteristics and performance of these methods in detail. Rather, we wanted to select two of the most promising methods and to evaluate them for our animal models: mouse tumor and cat brain hypoxia. Among the most desirable features of localization methods in decreasing order of importance are short acquisition time, high sensitivity, high spatial and spectral resolution, insensitivity to T_1 and T_2 relaxation time, and relatively simple implementation. The factors that affect the accuracy of localization (such as T_1 relaxation effect, tissue heterogeneity), signal-to-noise ratio, T_1 relaxation, and localized shimming will be discussed in detail in this chapter.

TABLE 3. CHARACTERISTICS OF B_1-GRADIENT LOCALIZATION METHODS

Method Number	1	2	3	4	5	6
MAIN AIMS						
speed	v		v			
sensitivity	v	v	v	v	v	v
spectral resolution	v	v	v	v	v	v
spatial resolution						b
several ROIs	d	d	d	d	d	d
one ROI	v	v	v	v	v	v
ROI near surface	v	v	v	v	v	v
ROI at depth						
SHAPE OF ROI						
slice						v
column						
cube						
SAMPLE LIMITATIONS						
very low sensitivity	e	e	e	e	e	e
very short T_2	v	v	v	v	v	v
very wide spectra	v		f	x		
aperiodic motion	v					
EQUIPMENT LIMITATIONS						
inhomogeneous B_0	v	v	v	v	v	v

v:fulfills a certain criterion
b:selects a slice only
d:with several surface coils only
e:only suitable for ROIs at surface
f:no statement available

method number 1 = SC (Surface Coil) [21]
2 = SC + phase cycling [22]
3 = SC + composite pulse [23]
4 = SC + pulse cycling composite pulse [20]
5 = SC + Fourier series window [24]
6 = Dress [25]

ISIS Localization

Introduction

For the cat brain hypoxia study, we have chosen the image-selected in vivo spectroscopy (ISIS) sequence, which has been adopted in most human in vivo spectroscopy investigations and some animal experiments (abstracts of the 1988 SMRM). We chose ISIS for the following reasons.

(A) A method is needed to localize the spectrum in a volume which can be reduced and enlarged and can be moved rapidly in space to investigate other volumes of interest within the sample, in this case, the cat's head. This requirement has ruled out the possibility of using a surface coil. The surface coil has two main disadvantages for studying the cat brain: (1) lack of penetration depth and (2) poor lateral localization. The surface coil localization is essentially in one spatial dimension, the one parallel to the B_1 direction, with the remaining two dimensions being localized by the diameter of the surface coil. Since the cat's head has a thick layer of muscle overlying the skull, a surface coil is very unsatisfactory. Images and associated ^{31}P spectra in Figure 6 done with a surface coil and a half-saddle coil clearly show the difference between the sensitive volumes of these two coils. The left panel shows the surface coil ^{1}H image and the ^{31}P spectrum obtained using the same coil with a single-pulse sequence. The nearly absent PDE signals and high PCr/NTP ratios indicate that a large

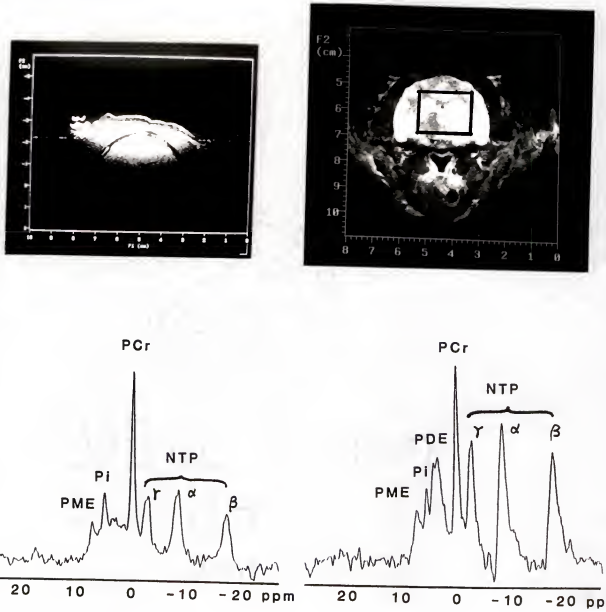

Figure 6. Effects of surface coil and ISIS localization. (a) ^{1}H spin-echo image and ^{31}P single-pulse spectrum using a 5-cm double-tuned flat surface coil. (b) ^{1}H spin-echo image and ^{31}P ISIS-localized spectrum using a 7.5-cm diameter double-tuned half saddle coil.

percentage of the signals came from the skull muscle. The right panel shows the half-saddle coil ^{1}H image and the ^{31}P spectrum using the same coil with ISIS sequence. A much higher PDE peak and relatively lower PCr/NTP ratios are an indication of good localization to the brain.

Some surface coil localization methods have the ability to suppress the strong signals from surface tissue, but this is done at the expense of either losing tremendous spatial sensitivity due to the characteristic of surface coil or reducing the filling factor and increasing the contamination from lateral direction when a large diameter surface coil is built to increase B_1 penetration depth. In ISIS, the selected volume may be easily moved in three dimensional space along any direction by either adjustment of the spatial position of the gradient zero-crossing point, or more conveniently, by adjustment of the RF frequency used during the slice selection. In this manner, the desired location for the selected volume may be encoded as three frequency offsets corresponding to the three spatial axes. The position of the selected volume can be determined by reference to the standard ^{1}H MRI.

(B) A method with no (or low) loss in sensitivity due to T_1 and T_2 relaxation and with the ability to measure T_1's and T_2's is needed. Considering that the T_1's of ^{31}P metabolites are on the order of seconds, (a typical set of T_1's are PME = 2.94s, Pi = 1.47s, PDE = 1.64s, PCr = 3.29s, γ-NTP = 1.36s, α-NTP = 0.97s, and β-NTP = 1.04s in the human brain [26];) a localization method which shows a slight T_1 weighting in the spectrum, on the order of

milliseconds, is tolerable. However, considering the T_2's of ^{31}P metabolites which are on the order of milliseconds (a typical set of T_2's are PMP = 84 ms, Pi = 62 ms, PCr = 169 ms, γ-NTP = 40.5 ms, α-NTP = 32.7 ms, and β-NTP = 27.2 ms in rat heart [27];) considerable losses in sensitivity are expected for compounds with short T_2 for methods which use echo techniques. This has ruled out the possibility of using some of the most commonly used methods such as PRESS [28], which use one 90° and two 180° selective pulses in the presence of magnetic field gradient (spin echo technique) to define a sensitivity volume and VOSY, which uses three 90° selective pulses in the presence magnetic field gradient (stimulated echo technique). The ability to combine the localization method with other sequences, such as inversion recovery sequence for T_1 measurement and spin echo sequence for T_2 measurement, are needed. T_1 can be measured with ISIS by varying the time delay between selective preparation and nonselective (with rectangular pulse) or selective (with adiabatic half-passage pulse) excitation. This delay is to allow for the decay of magnet eddy currents following gradient switching and can be as short as ~ 10 ms. T_2 can be measured with ISIS by adding a 180° nonselective pulse at the end of the sequence to produce an echo, which is a T_2-weighted signal.

(C) A method that can be applied with coils that show gross RF field inhomogeneity, such as surface coil, and cannot be affected in accuracy of localization due to inaccurate pulse tip angle and insufficient RF power. This latter consideration ruled out

techniques such as VSE [17]. If the pulse angle is not set up correctly, then the excited nuclei outside the VOI would give a much larger signal than those nuclei contained within the VOI. Insufficient RF, when a nonselective pulse is used in the presence of B_0 gradients, would cause serious off-resonance effect. In ISIS, inaccuracy in selective pulse tip angle, away from 180°, will not affect the cancellation of signals from external regions but will affect the signal-to-noise ratio, which can be compensated by increasing the number of averages. The errors in the cancellation process, which are mostly caused by spectrometer instability, have now been solved by the use of a selective noise prepulse [29].

(D) A method that can be extended to allow multiple volumes to be simultaneously investigated and conformed to fit the boundaries of an irregularly shaped anatomical volume more closely is desired. By additional selective RF pulses in the spatial encoding prepulse period [30] and by selecting more than three slices and turning on more than one gradient at a time [31], ISIS can achieve both goals mentioned above to produce improvement in the signal-to-noise ratio.

Methods

To evaluate the characteristics and accuracy of ISIS under extreme RF field inhomogeneity condition, a test had been performed on the 2T VIS spectrometer/imager in the following way. (a) A surface coil of 8-cm in diameter was first constructed

and double-tuned to ^{31}P (34.6 MHz) and ^{1}H (85.5 MHz) with the trap-circuit configuration [8] and matched to the phantom in (b). (b) A phantom consisting of two cubes with the small cube (2 cc), containing ~ 1 M HCCTP (6 M of ^{31}P) dissolved in benzene, sitting on top of big cube (70 cc), containing 0.2 M NaH_2PO_4 dissolved in water doped with 2 mM $CuSO_4$ for shortening relaxation time of ^{1}H ($T_1 \approx 200$ ms). (c) B_0 homogeneity was adjusted by shimming on the ^{1}H signal. Proton spin-echo 10-slice images in both transverse and sagittal directions (500/30) were obtained for the positions and sizes that are needed in the ISIS sequence. (d) A single-pulse sequence, with rectangular pulse, was used to set up 90° tip angle on the small cube (Figure 7(a)). (e) A single-pulse sequence at the ^{31}P frequency, modified by replacing the rectangular pulse with a selective "180° hyperbolic-secant pulse" of 5 ms duration (spectral width of 1600 Hz or 46 ppm for ^{31}P) was used to calibrate the transmitter power which yielded uniform 180° tip angle within the sensitive volume of the coil without applying B_0 field gradient (Figure 7(b)). Notice that a 180° tip angle is achieved by even further increasing transmitter power. The 90° adiabatic half-passage pulse can also be calibrated in the same way if the nonselective 90° excitation pulse, calibrated in (d) needs to be replaced. (f) Calibration curves, with gradient strength versus slice thickness for both ^{1}H and ^{31}P, were obtained experimentally by measuring the slice thickness in the imaging sequence in (c) by using both 90° and 180° adiabatic pulses in the presence of readout gradient. A calibration curve for H-1 is shown in Figure 8 and was

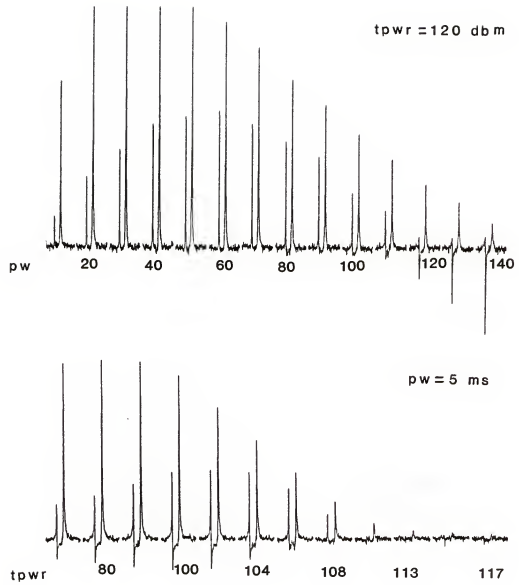

Figure 7. Tip angle calibration curve for (a) 90° hard pulse by varying pulse widths (10-140 μs) at fixed transmitter power and (b) 180° hyperbolic-secant pulse by varying transmitter power (70-117 dbm) at a fixed pulse width (5 ms). The 180° pulse is achieved when transmitter power exceeds 113 dbm. The left small peak is from HCCTP and right large peak from NaH_2PO_4.

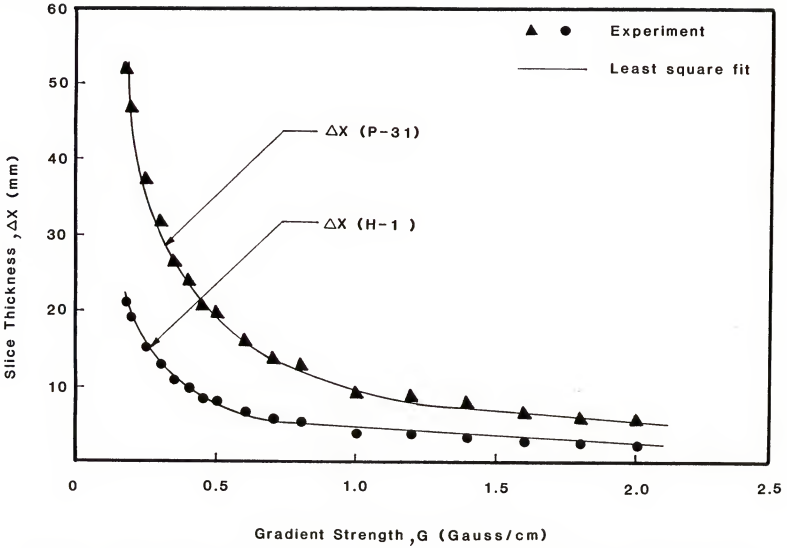

Figure 8. Calibration curves at ^{1}H and ^{31}P frequencies with gradient strength (G) vs. slice thickness (ΔX) for 5 ms hyperbolic-secant pulse width.

fit with the linear regression method. This curve matched very well with the curve calculated by the following equation: $\Delta X = 2\pi/\gamma \cdot \Delta f/G$ (ΔX = slice thickness, γ = gyromagnetic ratio, Δf = spectral width associated with 5 ms pulse, G = gradient strength) assuming Δf = 1600 Hz. Slice thickness for ^{31}P can be calculated by multiplying that of ^{1}H by 2.47 ($\gamma(^{1}H)/\gamma(^{31}P)$). (g) First, by using the of the small cube as the center of the VOI in ISIS and using the parameters obtained in (d) and (e), a series of spectra were obtained by increasing gradient strength (or reducing volume) according to Figure 8 or reducing volume, starting with zero gradient. A 15 ms delay between experiments was used for complete relaxation and localization.

Complete localization of signals from a small cube containing HCCTP is shown in Figure 9. Second, by moving the center of VOI to the center of the large cube, a series of spectra were obtained by the same procedure and are shown in Figure 10. We see complete localization in the large cube containing NaH_2PO_4 and signal-to-noise ratio reduction as the VOI's are reduced. In both Figures 9 and 10, the left panel shows the geometrical layout (cross sectional view) of the phantoms (solid line) and the surface coil. The various sizes of VOI's are shown by a dashed line. The right panel shows the ^{31}P spectra obtained from each VOI using ISIS. Decrease in NaH_2PO_4 signals (from the large cube) and constant HCCTP signals (from the small cube) and constant HCCTP signals (from small cube) are clearly seen in Figure 9 as the volume decreases when VOI's are centered at the small cube. Gradual decrease in the NaH_2PO_4

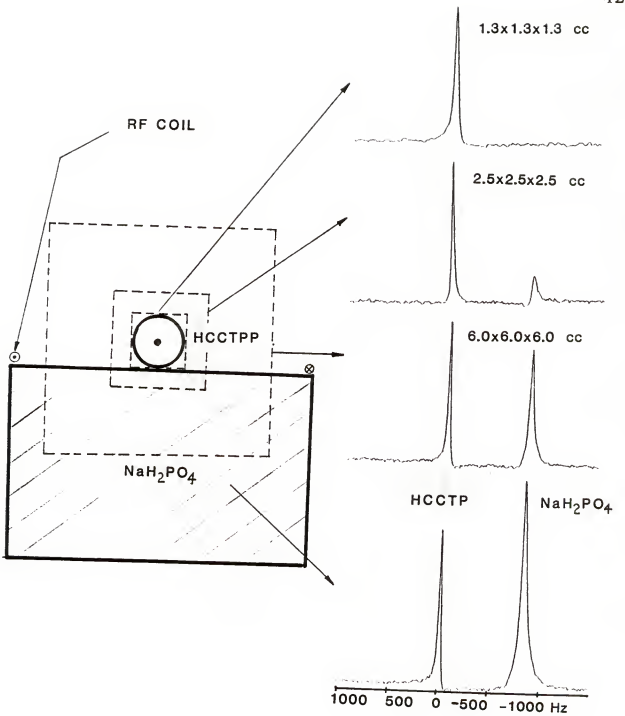

Figure 9. Demonstration of spectral localization using ISIS. Left panel: experimental setup of a 1.2-cm vial containing HCCTP on top of a 10-cm bottle with 8-cm diameter flat surface coil. Right panel: ^{31}P spectra from VOI's indicated with center at the vial.

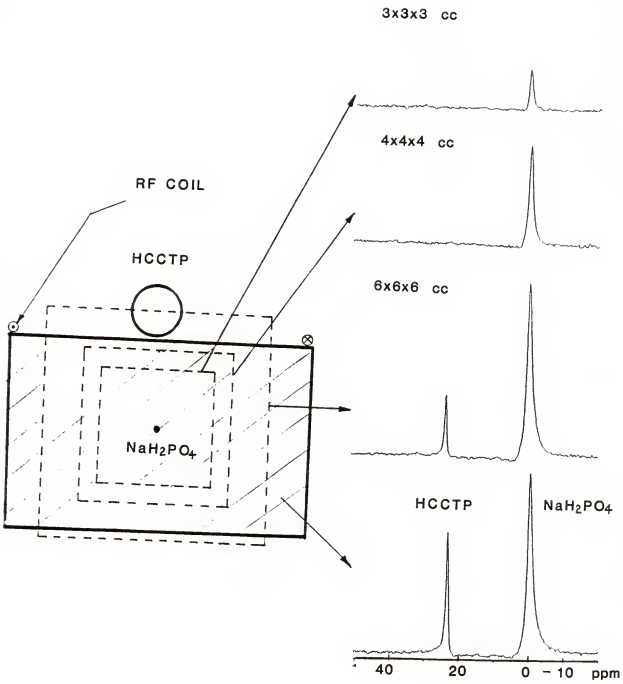

Figure 10. Same as in Figure 9 except with center of all VOI's at the center of the bottle.

signals and complete disappearance of the HCCTP signal are seen in Figure 10 as the volume decreases when the VOI's are centered at the large cube.

Discussion

This sequence has been used for the cat brain hypoxia study described in Chapter V. Although this method provides excitation of well-defined spatial planes for a single chemical shift, when many chemically shifted species are present, the frequency dispersion observed in the presence of gradients represents the combination of the spin distribution and the corresponding chemical shift dispersion. Under these circumstances, slice selection gives ambiguities in the spatial planes of the chemically shifted species excited by the frequency-selective pulse. This is called chemical shift displacement. The chemical shift displacement is given by $\Delta\chi = 2\,\pi/\gamma \bullet \Delta f/G$, where Δf is the chemical shift separation in hertz and G is the B_0 gradient strength in hertz/centimeter. At low fields (or small Δf) small gradients can be employed and $\Delta\chi$ will still be negligible compared with the slice thickness. However, at high fields, or large Δf, problems can be so severe that a completely different plane is excited. At a constant field in actual practice, the sensitive volume is localized accurately only when the B_0 gradients are strong compared to the width of the spectrum of the nuclei of interest. For a 2T spectrometer and a gradient strength of 0.5 Gauss/cm, the displacement caused by the

differences in chemical shift will be 2 mm for a ^{1}H spectrum with a spectral width of 5 ppm and 10 mm for ^{31}P spectrum with a spectral width of 25 ppm. It should be noted that the "displacement to slice thickness ratio" is held constant under a certain set of experimental conditions because increasing the gradient not only decreases the displacement but decreases the slice thickness. In this study, with B_0 = 2T, selective pulse bandwidth = 1600 Hz, the ratio is 0.54 which is very significant when accurate localization is needed. In the cat brain study, we had decided that the PCr and Pi signals (5 ppm apart) are the most important indicators of the degree of hypoxia. The displacement was only 2 mm (less than 10% of slice thickness) when the transmitter frequency was set on PCr. Improvement of this ratio can be done by using a selective pulse of wider bandwith (shorter pulse duration) in conjunction with a stronger gradient to reduce the displacement while maintaining the VOI.

Surface Coil Localization

The surface coil technique, first introduced by Ackerman et al. [20], has been used for localization in a variety of in vivo studies. We had adopted this technique in some of our mouse tumor studies. Because of the protruding characteristic of most of subcutaneously implanted tumors, this technique can provide localized detection of the tumor by avoiding signals from the surrounding normal tissues.

Eliminating signals from surrounding tissue is very important especially at early stage of growth, while the tumors are small.

One practical problem associated with this type of study is reaching a compromise between the B_1 penetration depth, which is approximately equal to the coil radius and signal contamination from the surrounding normal tissue. In order to reduce the signal contamination, the surface coil has to be placed some distance from the surface, so that only the tumor is included in the sensitive volume of the coil. However, this results in a loss of spatial penetration. Alternatively, a small surface coil (relative to the size of the tumor) can be used. This again has the possibility of nonuniform sampling of tumor tissue due to its lack of penetration depth.

To eliminate spurious signals from other parts of the body, a Faraday shield, which customarily consists of a grounded copper sheet with a hole to fit the size of the protruding tumor, is placed between the surface coil and the mouse. This method of using surface coil and the single-pulse sequence provides a simple method for studying subcutaneously-implanted tumors at early stages of growth when they are still responsive to therapy, and eliminates the need for magnetic gradients for localization. As the tumor grows, the relative positions of various regions within the tumor to the surface coil can change; therefore, the contributions of these regions to the NMR spectrum also vary. If this is the case, then it would be very difficult to distinguish between spectral changes due to changes of the metabolism of the tumor and changes due to sampling changes of various regions of the tumor.

Such sampling artifacts can be reduced or avoided by restricting these studies to histologically homogeneous tumors, i.e., tumors that do not present localized gross necrosis. The problem can also be minimized by using a solenoidal coil which can easily encompass protruding subcutaneous tumors. Here again, a Faraday shield (as described for the surface coil) can be used to eliminate spurious signals from adjacent normal tissues. A solenoidal coil can generate a more uniform B_1 field over most regions of the tumor.

In spite of its easy implementation and good filling factor, the use of the surface coil techniques is limited by its (1) crude localization in the lateral direction with ill-defined boundaries, (2) shape of the sensitive volume due to fast pulsing (see section "Relaxation Effect in Accuracy of Localization" in this chapter) and (3) applications when sensitivity near the surface is desired.

Relaxation Effect in Accuracy of Localization

When a T_2-weighted sequence is used, differences in T_2's, which cause different degree of irreversible loss of microscopic phase coherence between the spins in a specimen, can affect the signal intensities differently but not the spatial localization. However, difference in T_1's, which are a measure of how long the spin system takes to recover its equilibrium population distribution, will not only affect signal intensity due to saturation effect, but affect localization profiles of different spins due to the

inhomogeneous distribution of B_1 field within the sensitive volume. In other words, the sensitivity of the coil and its spatial localization depends on the T_1 of the metabolite under investigation. This can be a problem when dealing with several different metabolites or nuclides with distinct T_1's. Unfortunately, this effect affects most the simplest localization method, surface coil technique, because of the fast drop in B_1 strength along the axial direction. When the tip angle at the center of a surface coil, used as both transmitter and receiver, is adjusted to be 180° to suppress the surface signals, Figure 11 shows several axial sensitivity profiles of species with different T_1's according to the following equation for a single-pulse sequence.

$$S \propto (\sin \theta) \frac{1 - \exp(-T_r/T_1)}{1 - [\exp(-T_r/T_1)] \cos \theta} B_1 \qquad [32]$$

where S is the signal intensity, θ is the tip angle and Tr is the recovery time. As can be seen here, metabolites which differ in a factor of about three in T_1 (a range found in ^{31}P metabolites in biological systems), can have substantially different excitation profiles. Note that the major difference occurs near the coil, whereas nearly identical profiles are seen from the regions farther from the coil despite differences in T_1's. This effect, which differently saturates different species at different regions, requires great care when interpreting the results obtained with a surface coil. Fortunately, for localization methods using B_0 gradients and

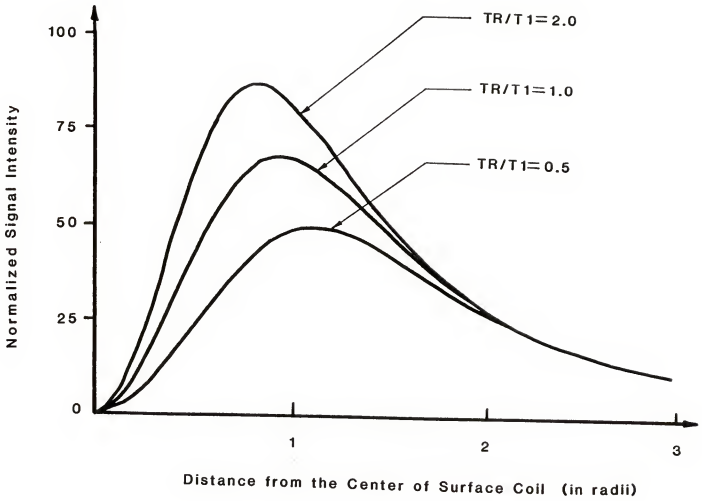

Figure 11. T_1 effect on surface coil localization with (a) $TR/T_1 = 2.0$, (b) $TR/T_1 = 1.0$, (c) $TR/T_1 = 0.5$.

selective pulses, especially with an RF coil which has a more homogeneous B_1 profile (such as half-saddle coil), the effect is much less severe when VOI's are small compared to changes in the B_1 field. If there is a substantial variation in the B_1 field over a VOI, then the same considerations apply as for the surface coil. In addition by the use of an hyperbolic-secant pulse to obtain uniform 90° excitation everywhere in the sample, this effect is even less severe because the longitudinal magnetization is zero following the pulse at every point in the sample. We note that the denominator in the equation above becomes 1.

Localized Shimming

Before a localized spectrum can be obtained either by using a surface coil or the use of selective pulses in conjunction with B_0 gradients, the main magnetic homogeneity (B_0 homogeneity) over the region of interest must be optimized. This is usually done by observing the free induction decay or spectral amplitude of ^1H as the shim settings are varied. We wanted to investigate whether it is enough to shim on the signal received from the entire sample (total shimming) using a single-pulse (nonselective or hard pulse) sequence or localized shimming using localized sequence even though it is likely that the degree of inhomogeneity decreases with decreasing volume due to smaller field variation within the volume. We also wanted to investigate the degree of difficulty to shim when the volume of interest is not in the center of the magnet (i.e., is

remote from the center of the shim coil set), as is often the case. This causes problems because the magnetic fields produced by the shim coils are only orthogonal over a spherical volume (sensitive sphere) centered on the center of the magnet and the shim coil set. Experiments were performed on the 2T VIS with the half-saddle double-tuned coil designed for the cat hypoxia project by shimming on H-1 signal. The phantom was a 7-cm diameter plastic ball filled with distilled water doped with copper surfate to shorten T_1 ($T_1 \equiv 200$ ms). This experiment was divided into two parts. The first part was done by shimming the entire sample with the single-pulse sequence and by measuring a series of line widths (full width at half maximum height or FWHM) with increasing gradient strengths (decreasing in volume) and without changing the centers of the volumes using ISIS. These data are compared with line widths associated with the same volumes except shimming separately with the VOSY sequence. An in vivo experiment was done on a cat's head by total shimming of the head. Line widths from the entire head and from selective volumes of different sizes with the center remaining unmoved within the brain were recorded to estimate the relative effect of volume size and tissue susceptibility on B_0 inhomogeneity. The second part of the experiment was to measure a series of line widths of a selective volume with a fixed size as its center was moved away from the center of the magnet and to compare with those that were shimmed separately with the same sequence at each movement. Total shimming was done five times. After each shimming was

completed, the line width was measured. Three repetitions were done for localized shimming. Averages of the measurements are used in the following figures.

Figure 12(a) shows the comparison between total shimming and localized shimming. The value presented is an average of 5 measurements for total shimming with a standard error <5% of the mean and 3 measurements for localized shimming with a standard error <7% of the mean. For both total and localized shimming, the results show a significant decrease in linewidth only when the selective volume is a small fraction of the entire volume within a homogeneous sample. No significant differences are shown between localized shimming and total shimming. The in vivo data show a sudden decrease in linewidth when the volume of interest is completely localized within the brain, in contrast to the entire head which contains muscle, bone, brain, oxygen tubings, and air cavities (sinus, ear, etc.). Once the volume is within the brain, not only no further decrease in linewidth is shown, but somewhat of an increase when the volume covers a large portion of the ventricle where volumes are extremely heterogeneous.

Figure 12(b) shows the effect when volumes of interest chosen with the object are off center while the object was placed in the center of the magnet. The linewidth increases gradually for about 2.5 cm off center and then more noticeably outside that range. Localized shimming can improve the linewidth within the same range; however, once it is outside the range, no shimming is

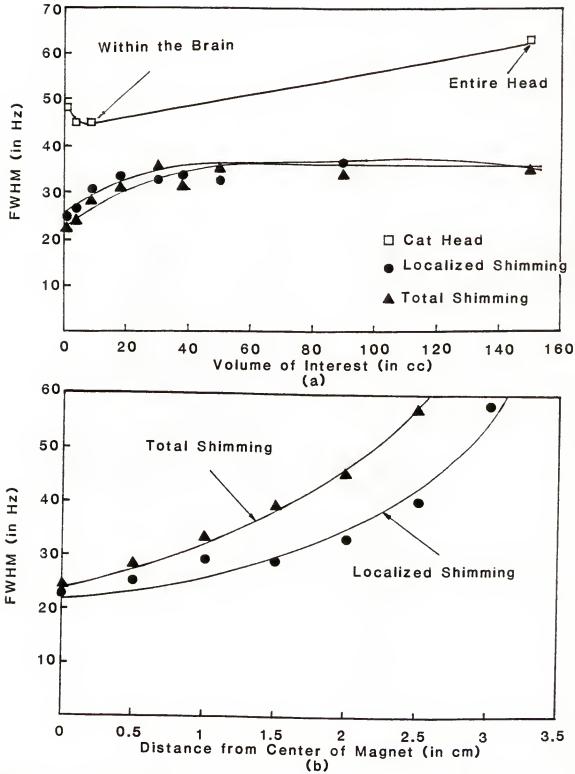

Figure 12. B_0 homogeneity adjustment with and without localized shimming in phantom and in vivo with center of VOI's (a) centered and (b) off-centered of the magnet.

possible. Movement in all three directions (x, y, z) was done and showed the same results.

From the data shown in Figure 12 and our experience in shimming, we can come to the following conclusions. (a) Neither total shimming nor localized shimming is possible when the volume of interest is outside the sensitive sphere which has a size depending on the magnet specification. (b) Localized shimming can certainly improve linewidth when the volume of interest is off-center but still within the sensitive sphere. (c) Even though reduction in size of volume of interest does improve linewidth within it, it is the susceptibility that is limiting the possible degree of improvement. (d) No localized shimming is needed within a homogeneous sample since linewidth decreases automatically as volume decreases. (e) The above conclusions are suitable for a coil with relatively uniform B_1 field. In the case of a surface coil, most of the signal in shimming comes from the part of the sample that is close to the coil where B_1 intensity is stronger and, therefore, more sensitive to shim setting changes. The linewidth obtained is a compromise between the degree of off-center of the volume of interest and the distance from the coil. This is confirmed by the following observation. When a 10-cm diameter flat surface coil was used on top of a cat's head, ~ 35 Hz linewidth was obtained by total shimming the entire sensitive volume which covered only the top part of the head (see Figure 6(a)). When an 8-cm diameter half-saddle coil was used, ~65 Hz linewidth was observed due to a much larger field of view which covers the entire head (see Figure 6(b)).

However, ^{31}P spectra from a selective volume of 8 cc with ISIS sequence in the brain showed almost identical spectral resolution (linewidths of PCr were ~ 20 Hz with 10 Hz line broadening) in both cases in spite of the large difference in linewidth with total shimming. (f) Sometimes, shimming is considered an art rather than science when manual shimming is used. This is not true, in our experience, when the protocol for shimming provided by the manufacturer is closely followed. Good B_0 homogeneity can be achieved without having too much difficulty. In shimming, both the time domain signal (free induction decay or echo) and frequency domain signal (spectrum) are needed for the evaluation of field homogeneity. The former is used to monitor the duration of the exponential decay (T_2^*), and the latter to see the changes in line shape.

Fractional Tissue Components

Almost all of the proposed localization methods using B_0 gradients with selective pulses, such as ISIS, can accurately select VOI's within the tissue by reference to an MRI image. MRS signals are useful for the study of volumes of tissues that are reasonably homogeneous, such as liver, skeletal muscle, etc. For organs such as brain and kidney, which are less homogeneous, physicians will be more interested in analyzing specific types of tissue rather than the combinations of several different tissue components that may be present in the VOI. For example, ^{31}P spectra from the cat brain

we obtained by using ISIS, Figure 13, suggests that gray matter has different phosphorus metabolite concentrations from white matter.

Present localization techniques do not allow these two components to be measured separately. We propose a method here that can lead to the separation of such components. We note that image-guided localization methods not only provide positions and sizes from which the localized spectra are acquired, but provide information about the fractional volume of each particular type of tissue within the VOI if different tissues are well differentiated in an image [33]. We propose a simplified mathematical model which provides a solution for the problem stated above. We make the following assumptions: (1) homogeneous B_1 profile (i.e., homogeneous transmission and reception within the VOI's), (2) metabolite concentration of any particular type of tissue remains a constant throughout the VOI's and during the sampling time.

Since a spectrum in the frequency domain can be represented by a set of coefficients, $A_n(k)$, the equation can be expressed as

$$S_m(k) = \sum_{n=1}^{N} V_{mn} A_n (k)$$

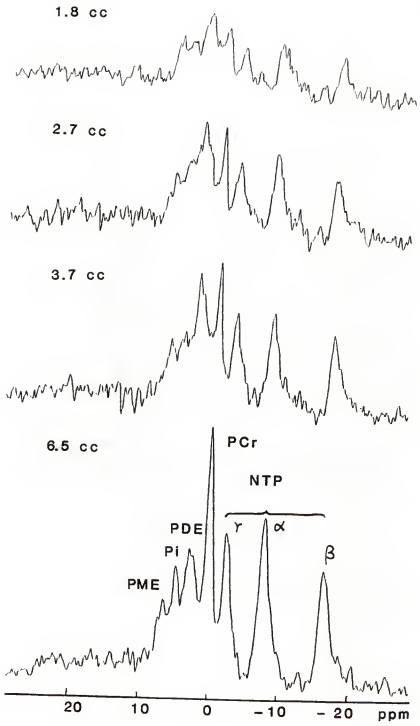

Figure 13. ^{31}P spectra from VOI's of different sizes centered at the third ventricle in the cat brain--A demonstration of fractional tissues effect.

$(1 \leq k \leq K)$ where K = the total number of points representing the spectrum

$(1 \leq m \leq M)$ M: number of linearly independent measured spectra

$(1 \leq n \leq N)$ N: total number type of tissues under investigation

$S_m(k)$: signal intensity, in the frequency domain, of the k^{th} point in the m^{th} spectrum

V_{mn}: the total volume of the n^{th} type of tissue present in the m^{th} spectrum

$A_n(k)$: signal intensity, in the frequency domain, of the k^{th} point from the n^{th} type of tissue.

This equation represents a linear system of equations and can be solved exactly, if $M \geq N$, by standard numerical methods such as the Gauss-Jordan Elimination Method, at each frequency for the unknown $A_n(k)$ which yields spectra from each particular tissue. The major advantage of this method is that good signal-to-noise ratio is obtained without having to reduce the VOI in order to fit it nearly within the desired volume of tissue. Condition (1) can be achieved or compensated for by either using hyperbolic secant pulses for uniform transmission and B_1 field plot for calibration in reception. The major source of error will come from condition (2) which may not hold for pathological conditions. Other sources of

error depend on how well a spectrum is digitized, how well different tissues can be differentiated which lead to associated volumes be measured. So far, we have not done anything as far as experiment. Instead, we are proposing here a possible solution for improving localization of heterogeneous tissues.

CHAPTER IV
RADIO FREQUENCY COILS FOR ^{31}P MRS IN VIVO STUDIES

The Importance of and Requirements for RF Coils

It is almost impossible to overestimate the importance of properly-designed radio frequency (RF) coils, for transmission and receiving, in MRI and MRS. In MRI, a "high-quality" RF coil is needed to provide good sensitivity and improve spatial resolution in the image, especially of small organs of the human body. In MRS, the coil is needed to excite nuclear magnetic spins either within the sample in a spectroscopic imaging experiment or a particular localized volume of interest in a living system. The coil also detects the NMR signals, which are then processed to provide a spectrum. To obtain ^{1}H images and then localized spectra of other nuclei, an efficient coil setup is needed. This can be either a set of coils tuned to different frequencies and positioned properly or a multiply-tuned coil. It has been suggested that two separate coils, such as a volume coil for ^{1}H MRI and a surface coil for ^{31}P MRS be used together. The problem is that when two (or more) coils, even though tuned to different frequencies, are used in close proximity, they couple. That is, the RF field of one coil induces an alternating

current in the second coil which will in turn produce another RF field opposed to the first RF field. It is generally assumed that when two coils are orthogonally arranged, the coupling effect can be eliminated. We had tested this scheme by making the B_1 of a flat, circular surface coil, tuned to ^{31}P frequency for transmission/receiving, orthogonal to that of a volume (saddle) coil, tuned to ^{1}H frequency for transmission/receiving. We found, from images, that the RF field homogeneity of the volume coil is greatly degraded by the presence of the surface coil. We expected the same to be true for the surface coil due to the mutual coupling. This is a somewhat surprising result, which makes the RF field unpredictable. It cannot be compensated by this decoupling scheme. The foregoing considerations raise the need for a multiple-tuned coil which can be used when operating the spectrometer at more than one frequency without changing coils during the experiment. In addition, since ^{1}H-^{31}P spin-spin coupling effect (coupling constant = 5-10 Hz) is responsible for a large part of the loss of spectral resolution in in vivo ^{31}P MRS, heteronuclear decoupling techniques (such as ^{1}H-decoupled ^{31}P MRS) are urgently needed to improve existing localization techniques in order to enhance spectral resolution. A double-tuned coil can therefore provide the need for this type of application. A double-tuned coil is also needed when shimming is done with the ^{1}H signal and spectroscopic measurement is done on another nucleus of interest, such as ^{31}P. It is possible to shim on a coil <u>not</u> tuned to ^{1}H. This is because the concentration of water is so high that

sufficient ^{1}H signal can be detected with a coil that is not tuned to ^{1}H frequency. However, B_1 intensity is so small on a coil not tuned to ^{1}H in most of the sensitive volume of the coil that the bulk of signal is from the small regions immediately adjacent to the coil. Shimming is therefore performed on these regions rather than on the bulk volume of the sample. This results in the B_0 homogeneity remain very poor over the total volume of interest.

Several methods for double-tuned coils have been proposed to achieve this purpose. Unfortunately, none of these methods can be used without losing sensitivity due to circuit loss, such as (a) increase in reactive components due to the use of a transmission line for tuning [34], (b) reduction in coil sensitivity at the frequency that uses the transmission line to tune outside of the sample [35], (c) reduction in coil sensitivity due to extra use of inductive components [10], and (d) reduction in coil sensitivity in counter-rotating current mode due to close coupling [36, 37]. Other requirements and considerations for double-tuned coils are the following: (a) no or low loss of sensitivity in the low-frequency mode when nuclei at this frequency have low NMR sensitivity and natural abundance, (b) the degree of difficulty to build the coil, (c) the possibility of double-tuning the coil with two frequencies of interest closely spaced (for example, 85.5 MHz for ^{1}H and 80 MHz for ^{19}F; 26.7 MHz for $^{13}C$and 28.1 MHz for ^{23}Na), (d) the possibility to obtain absolute molar concentration measurements. It is the purpose of this study to evaluate three coils that have been described in the literature by Fitzsimmons [36], Rajan [37], and

Schnall [10]. We want, first, to understand the operational characteristics, second, to evaluate their performance at both low and high frequencies by comparing with single-tuned coil of the same size, and, third, to choose the coil that is most appropriate for in vivo MRS.

Coil Design Theory

The transformer-coupled double-tuned coil by Fitzsimmons [36] utilizes a high degree of coupling between the primary and secondary circuit in a double-tuned circuit. Two resonance frequencies are produced due to a high coupling constant, which also determines the separation in frequency. A vector analysis of the circuit, shown in Figure 14(b), had shown that the current L_1 and L_2 are in phase below the pole frequency and 180° out of phase above the pole frequency. Since the B_1 field strength is proportional to the vector sum of the currents in L_1 and L_2, the out-of-phase current in L_2 causes the B_1 fields from L_1 and L_2 to oppose each other. This not only means a loss in efficiency at high frequency, but two different B_1 profiles for two frequencies. Analysis further shows that, due to the symmetric property of the linear system equations associated with this circuit, two resonance frequencies will be created in this circuit. This means that a multiple-tuned coil can be easily made in theory simply by adding loops. We had successfully made a triple-tuned coil of frequencies 22 MHz (^{23}Na), 34 MHz (^{3}P), and 85 MHz (^{1}H) according to this circuit.

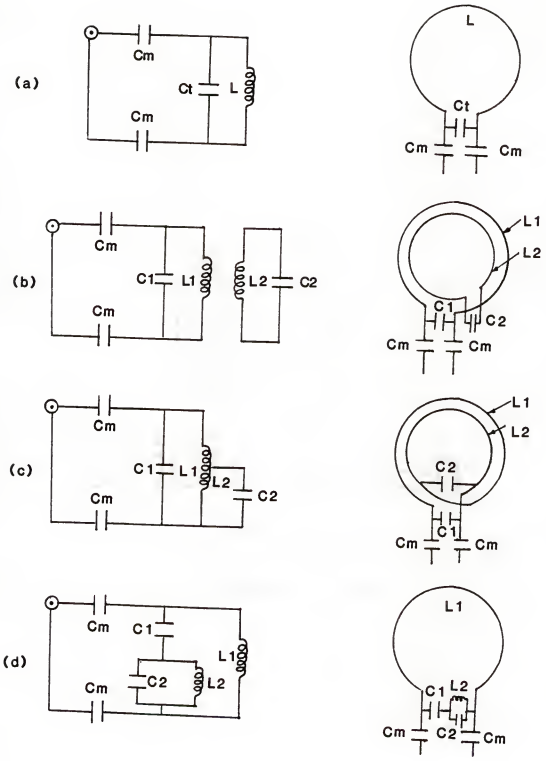

Figure 14. Resonance circuits of a single- and three double-tuned coils (left panel) and their associated configurations (right panel): (a) single-tuned, (b) Fitzsimmons, (c) Rajan's, and (d) Schnall's double-tuned coils.

A very similar but even more closely coupled double-tuned coil was proposed by Rajan [36]. One major advantage of this design is the simplicity of construction. By only adding a shunt capacitor which tends to minimize the circuit loss due to the use of a single inductive element in some cases. However, because of the very high coupling constant, this technique not only cannot be tuned to two frequencies which are closely spaced, but also minor tuning adjustment on one frequency affects the tuning of the other. This can make the tuning process to adjust for loading effects a very time-consuming process. Different B_1 profiles at each frequency due to the out-of-phase in currents in L_1 and L_2 are the same as in the transformer-coupled coil described above. Because of the lack of flexibility of matching the high frequency to the sample load, a lower efficiency for the high frequency is expected for this coil compared to the transformer-coupled coil. Figure 14(c) shows the Rajan design and its actual coil configuration.

The trap-circuit, Figure 14(d), for double tuning coils was proposed by Schnall [10]. By using an additional pair of inductive and capacitive components, a second resonant frequency is created. For the previous two coil designs the high frequency losses are related to the frequency difference of the two frequencies. The high frequency loss is ~50% for a coil tuned to 34 and 85 MHz, and is ~65% for one tuned to 22 and 34 MHz. For the Schnall coil, the losses are inversely proportional to the inductance of the trap circuit. Although the losses in the low frequency can be minimized by minimizing the trap inductance, the relation between

low-frequency efficiency and trap inductance is not a linear relationship. Therefore, high-frequency efficiency can be optimized without losing that of low frequency. Other advantages are the following: (a) weak coupling between the two resonant frequencies makes it extremely easy to build the coil as well as tuning it; (b) weak coupling between the high frequency and sample is such that almost no adjustment is needed for loaded and unloaded conditions; (c) while the loading effect is the same on the low frequency as in a single-tuned coil; (d) the design can easily be extended to triple-tuned coil by adding another trap circuit. The major disadvantage is that the weak coupling between the trap-circuit and sample will reduce the efficiency in the high frequency mode.

Method of Comparison

Coil comparisons were performed on a 2.0 T SIS spectrometer/imager. The three double-tuned coils described above and a single-tuned coil, tuned to 34 and 85 MHz at a time, were built with identical shape, size, material, and components. All coils were flat, circular (4.3 cm in diameter) surface coils made with solid copper wire (1.2 mm in diameter) and were attached to a thin sheet of printed circuit board. Fixed-value capacitors and variable capacitors were used for tuning and matching. To minimize dielectric loses, all coils were balanced-matched to 50 ohms for both frequencies. The transformer-coupled coil was made

by tuning the low-frequency loop (outer loop) first, then the high-frequency loop (inner loop). A trial-and-error process is needed to achieve the wanted frequencies. Matching is done by the same process, since the capacitance for matching also affects both frequencies. For the transformer-coupled design, no capacitor is used between the primary and secondary loops for possibly better matching in the high-frequency mode. Rajan's coil is made by first single-tuning the circuit to low frequency on a two-turn coil, then a capacitor is connected across only one turn to create the high frequency. Again, due to the heavy coupling, the tune and match condition on both frequencies had to be achieved by iteratively changing the value of the tuning and matching capacitors. Changes in matching capacitors had even more of an effect on tuning frequencies than in a transformer-coupled coil.

The trap design coil was made by first tuning and matching the coil to the low frequency, as in a single-tuned coil, and then inserting the trap circuit with the smallest possible inductance, tuned and matched to the high frequency. This coil was tested on the spectrometer with a phantom described below for pulse widths to achieve 90° tip angle for both frequencies at the center of the coil. Inductance was then gradually increased by adding more turns of copper wire (0.5 mm in diameter) in the trap circuit, and each time the same measurement was repeated until the pulse width in the lower frequency started to increase (or efficiency started to drop) and that in high frequency was minimized (or efficiency maximized) as shown in Figure 15(a). Any time the inductance was

added to the trap circuit, no change in coil Q was found on either frequency. However, as predicted, the Q damping in lower frequency due to sample loading is much larger than in the high frequency as shown in Figure 15(b). The solid lines in each graph were fitted to all the data points by a linear least squares method. Each coil was tuned and matched by using a sweep generator (Wavetek) and a bridge circuit of 50 ohms.

To test the four coils in the spectrometer, a rectangular phantom (10 x 10 x 5 cm^3) filled with 0.9% sodium chloride solution and 0.1 M sodium phosphate was used to load the coil, and a microsphere of volume about 1 cc containing 6 M of HCCTP for ^{31}P and benzene for ^{1}H (which have NMR characteristics described in Chapter II) was placed in the center of each coil. To determine and compare the efficiencies of power delivery to the coil, the 90° pulse widths with respect to ^{31}P and ^{1}H were measured at the center of the coil using the signal originating from the microsphere. Signal-to-noise ratios were measured as the ratio of the peak height of ^{31}P in HCCTP to root-mean-square (rms) noise multiplied by the line width (in Hertz) for ^{31}P and that of the peak height of C-H resonance in benzene to rms noise multiplied by line width (in Hertz) at half height. The quality factor Q of each coil was measured using the reflected power detected from the same sweep generator and an oscilloscope and was calculated by taking the ratio of each resonance frequency to the bandwidth at 0.7 of the peak height under both unloaded and loaded conditions.

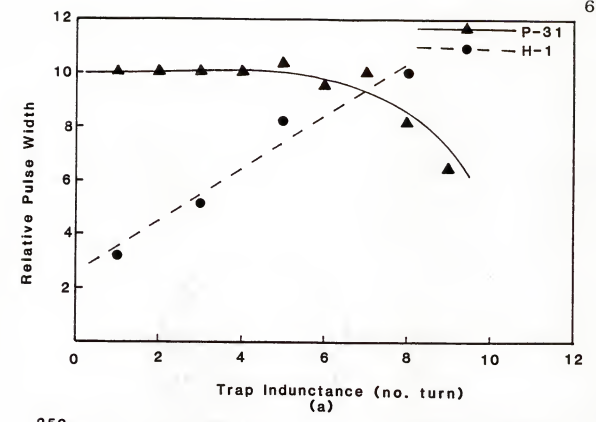

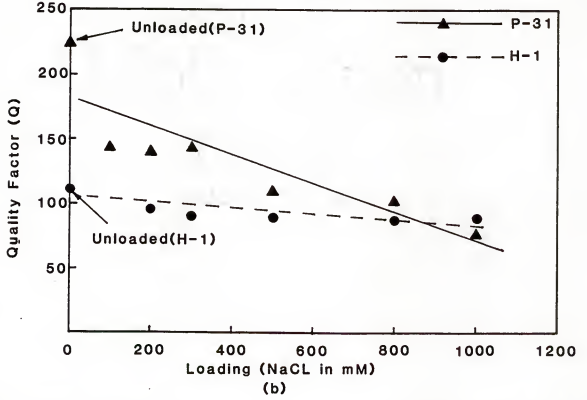

Figure 15. Characteristic curves of Schnall's double-tuned coil. (a) Efficiency curves with pulse width vs. inductance in the trap circuit. (b) Q changes due to various loading effects with NaCl concentrations (in mM).

Results and Discussion

Table 4 lists the coil performance of all three double-tuned coils and a single-tuned reference coil. The value listed is an average of 10 measurements with standard error <5% of the mean. In the low-frequency mode (34.6 MHz), the transformer-coupled coil and trap-circuit coil showed over 90% efficiency of power delivered as compared with a single-tuned coil, whereas Rajan's coil showed only 70% efficiency. However, all three coils gave very similar performance in S/N ratio measurement. In the low-frequency mode, no relationship was found between the ΔQ and efficiency (which is inversely proportional to pulse width) or S/N ratio measurements. Other researchers have claimed that ΔQ is an indication of coil performance. In the high-frequency mode, the trap-circuit design showed the highest efficiency of over 60% after optimization, whereas the transformer-coupled coil showed about 50% efficiency. Again, Rajan's coil had the lowest efficiency of 43%. A proportional relationship between pulse width and S/N ratio had been found; i.e., the shorter the pulse width, the higher the S/N ratio. Surprisingly, an inverse proportionality relationship had been found between ΔQ and efficiency.

Although the pulse width, which is a measurement of the intensity of the B_1 field, tells us how efficiently the power is delivered to the sample, it really is the S/N that we are mostly concerned about in an NMR experiment. All three coils gave similar performance of S/N in the low-frequency mode. The

TABLE 4. COIL PERFORMANCE COMPARISON OF THREE DOUBLE-TUNED COILS WITH SINGLE-TUNED COIL.

Coil	Q [unloaded]		Q [loaded]		ΔQ		90° pulse width		S/N	
	^{31}P	^{1}H	^{31}P	^{1}H	^{31}P	^{1}H	^{31}P	^{1}H	^{31}P	^{1}H
Single-tuned coil (^{31}P)	213		117		96		28 (100%)		90	
Single-tuned coil (^{1}H)		250		110		140		50 (100%)		73
Transformer-coupled coil	246	150	103	102	143	47	30 (93%)	102 (49%)	84	38
Rajan's coil	201	130	86	74	115	56	39 (71%)	117 (43%)	80	30
Trap-circuit coil	223	110	108	89	115	21	31 (91%)	79 (63%)	83	54

The value listed is an average of 10 measurements.
$Q = f/\Delta f_{0.7}$, f resonance frequency, $\Delta f_{0.7}$ frequency bandwith at 0.7 peak height.
ΔQ = Q (unloaded) - Q (loaded).
90° pulse width at the center of the coil (μs).
S/N = (peak height x line width) / γms noise.
( ) = percentage efficiency compared with the single-tuned coil.

trap-circuit design, which has the weakest coupling between the two frequency modes and between the coil and the sample, showed the best performance, even though it has the lowest Q and smallest ΔQ, in the high-frequency mode. This may nor may not be a significant factor in a particular experiment. It depends on whether the elongation of data acquisition (such as proton imaging) in the high-frequency mode to obtain a similar S/N ratio poses a problem.

Other observations in this study are the following: (a) Both S/N and pulse width measurement (or an equivalent method) are necessary for coil performance evaluation, since they do not necessarily linearly relate to each other. This is due to other possible contributions to noise in the circuit. (b) Coil quality factor, which is a combination of circuit Q and other factors such as quality of circuit component, does not seem to be an indicator of how good the S/N ratio will be. The possible reason for this may be that other mechanisms are dominating the dielectric loss. (c) The ΔQ does not serve as a good indicator of coil efficiency when coils are compared with different degrees of coupling between the low-frequency and high-frequency mode and different degrees of coupling between the high-frequency mode and the sample. A possible reason for this may be that the frequency-to-frequency coupling is dominating the sample-coil coupling. A coil with weak sample-to-coil coupling does not necessarily mean worse overall coil performance. This may be due to possible compensation from smaller magnetic losses, that is, eddy current dissipation power.

In conclusion, the trap-circuit design has been chosen for both the cat hypoxia and the mouse tumor study for the following reasons: (a) It gives similar S/N in the low-frequency mode and better in the high-frequency mode; (b) it is easy to build by inserting a trap-circuit in a single-tuned circuit with small resonance frequency shift in the primary loop; (c) it is easy to tune between two frequencies due to weak frequency-frequency coupling under different loaded conditions; (d) it is easy to extend to multiple-tuned coil, and, most of all; (e) in both frequency modes, it has the same B_1 profile without encountering a counter-current situation. This is a requirement for absolute molar concentration quantitation, which was described in Chapter II.

CHAPTER V
IN VIVO ^{31}P MRS OF MOUSE-TUMOR AND CAT-BRAIN HYPOXIA

In Vivo ^{31}P MRS of Human Osteosarcoma in Nude Mice

Introduction

A somewhat new area that is worth extensive investigation is the detection, differentiation, and prognostic prediction of malignant tumors using ^{31}P surface coil spectroscopy. This is accomplished by making noninvasive in vivo measurements of several important phosphorus metabolites including PCr, Pi, NTP, PME and PDE, as well as tissue intracellular pH. In the studies of malignant tumors in animals and humans, significant changes in ^{31}P spectra have been demonstrated during untreated tumor growth or treatment with chemotherapy or radiation therapy [38]. Although many types of tumors have been examined, the major difference between ^{31}P spectra of different tumors were either the presence or absence of individual tumor markers or the difference in ratio of ^{31}P metabolites. These findings, however, were a mixture of various types of tumors and characteristics of different stages of them. Due to the considerable controversy over whether each tumor type has its own characteristic ^{31}P spectrum, the most reliable and

comprehensive way to characterize them is to study each individual tumor type rather than trying to draw a conclusion using data obtained from other tumor types.

Osteosarcoma is the most common of all the primary osseous malignant bone tumors (~ 28%). Chemotherapy has contributed substantially to the control of metastases and the management of bone tumors. However, the cure rate for osteosarcoma in man is only 65-70% in five-year survival, with 30% mortality due to drug resistance. More biomedical information concerning the response to chemotherapy of both drug-sensitive and drug-resistant osteosarcomas in a controlled manner is urgently needed before any patient studies are attempted. Once a better understanding is obtained, it may lead to better patient management, such as type, dose, and timing of the administration of chemotherapy drugs.

It was the purpose of this study to characterize osteosarcoma using ^{31}P MRS at different stages of growth, to evaluate the sensitivity when a 2T spectrometer and surface coil are used and to optimize NMR parameters such as TR.

Methods

Female nude mice, each weighing 25-30 grams, bearing human osteosarcoma were used for these experiments. The tumor cells were obtained from Dr. B. Croker, Department of Pathology, University of Florida, in culture. Tumor cells (1×10^7 cells in a balanced salt solution) were induced by intradermal injection in the

gluteus maximus of the nude mice. NMR measurements were done on day 0 (before tumor cell implantation), 7, 15, 19 and 25 until tumors had reached a volume of approximately 1 cm^3. Mice were anesthetized by i.p. injection of INNOVAR/saline (0.4-0.5 cc per mouse with 1 part INNOVAR by Pitman-Moore Inc. and 9 parts normal saline), then were allowed to rest with light warming for 15 minutes prior to being put in the magnet for NMR measurements. This allowed, as shown by previous studies [39], full recovery of mouse blood pressure, heart rate due to the effect of anesthetics and, presumably, yielded a ^{31}P spectrum not influenced by these variables. Tumor volume was estimated by measuring the tumor dimensions along the long axis (height) of the tumor and across the tumor at the widest point (width). Tumor volumes were calculated by the equation [40]:

$$\text{Volume} = 0.5\ (\text{height} \times \text{width}^2)$$

In vivo ^{31}P MRS was done using a 2T SIS Inc. model VIS spectrometer equipped with a SUN-3/160 computer. A home-built probe containing 2-turn surface coil with a diameter of 1 cm was used. The coil was doubly tuned [10] to ^1H for shimming and to ^{31}P for data accumulation. The coil was carefully characterized for 90^o tip angle for ^{31}P (with pulse 5 μs at 110 db power) at the center of the coil with a microsphere containing ~ 6 M HCCTP. However, a long pulse width (8 μs) was used to obtain the signal from within the tumor and to avoid contamination from the skin. A short

repetition time of 1 sec was used to preferentially saturate the PCr resonance and the PME and PDE resonances. This was done so as to preferentially enhance the Pi resonance, so that the pHi measurement could be improved. Every mouse was marked on the tumor site for placing the surface coil with consistency. A copper Faraday shield was used to avoid contamination of signals from the surrounding tissue. Each spectrum was obtained by a total of 512 scans, with 5000 Hz spectral width and 2048 data points. ^{31}P chemical shifts are reported relative to the PCr resonance. PCr is present in all spectra and its chemical shift is pHi-independent and Mg^{+2}-insensitive. pHi was calculated from the chemical shift difference between PCr and Pi resonances (ΔPi in ppm) by the following relation [41]:

$$pHi = 6.72 + \log [(\Delta Pi - 3.27) / (5.69 - \Delta Pi)]$$

Each FID was processed with 20 Hz line broadening, and spectral baselines were corrected by convolution difference (~ 500 Hz) to eliminate the broad component from phospholipid which is commonly present in in vivo ^{31}P spectra. Because of similar ^{1}H linewidth at FWHM (~ 20 Hz) and similar sampling volumes, peak height of each resonance in a ^{31}P spectrum was used to calculate metabolite concentrations.

Figure 16 shows examples of the ^{31}P NMR spectra obtained from two mice (#1, #2) during untreated growth between day 0 and day 25 after inoculation. Figures 17-19 show the changes in tumor volume and metabolite content as the tumors grew. The size of the

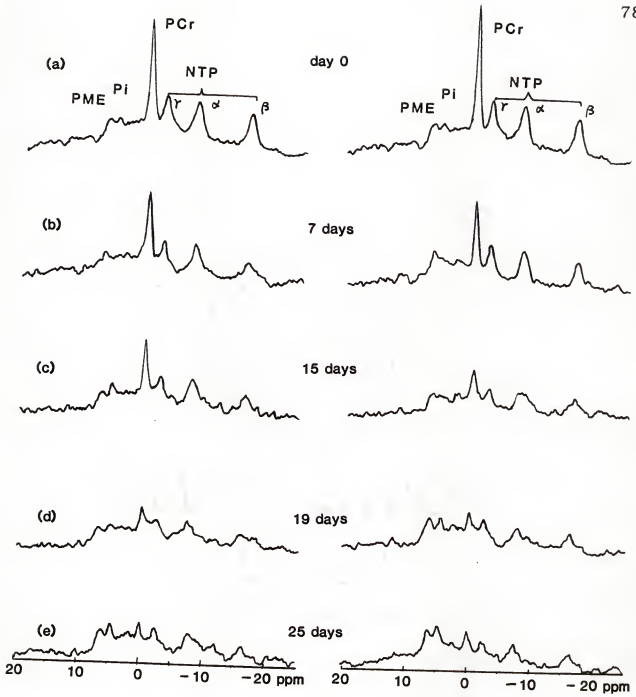

Figure 16. Typical ^{31}P spectra of subcutaneously implanted human osteosarcoma in nude mice during growth. Left panel shows spectra from mouse #1, right from mouse #2: (a) day 0, (b) 7 days , (c) 15 days, (d) 19 days, and (e) 25 days after implantation.

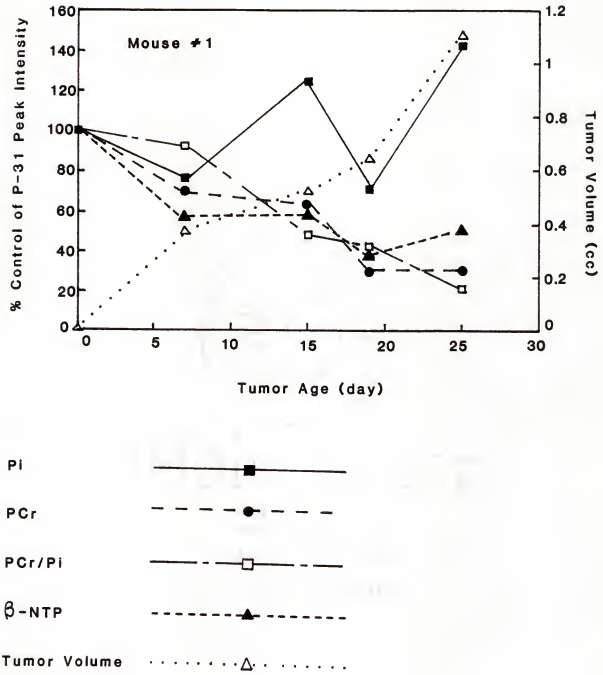

Figure 17. Changes (% control) in tumor volumes and ^{31}P intensities of osteosarcoma in mouse #1 during untreated growth.

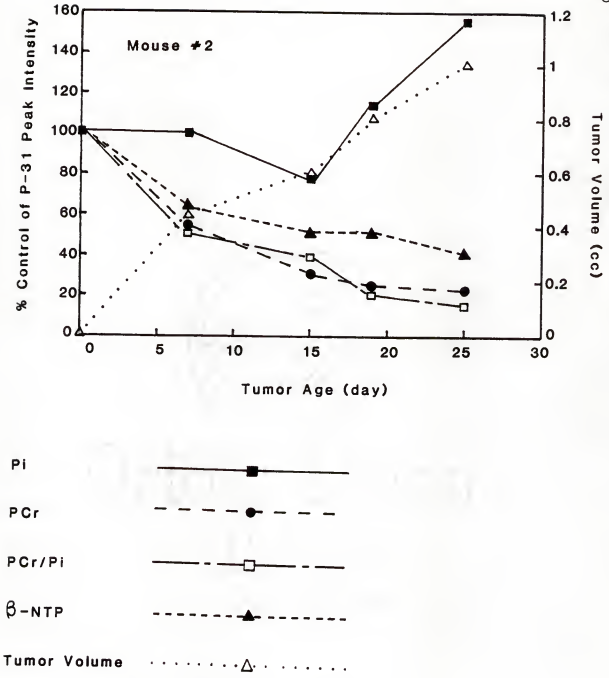

Figure 18. Changes (% control) in tumor volumes and ^{31}P intensities of osteosarcoma in mouse #2 during untreated growth.

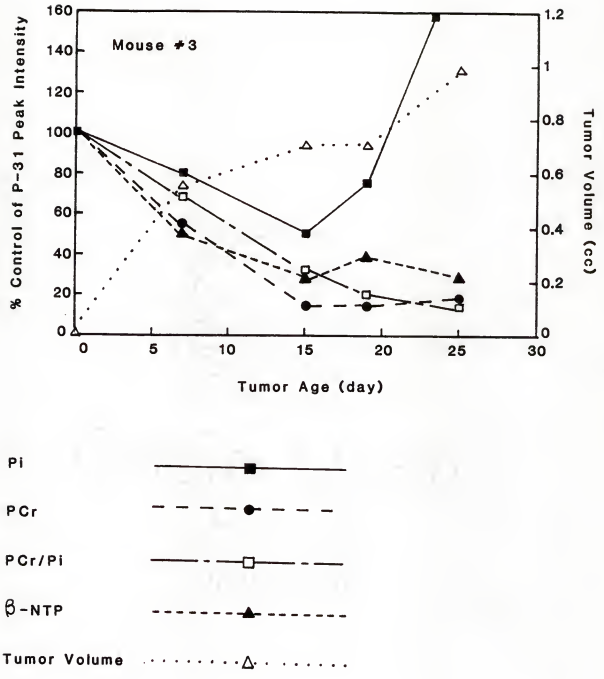

Figure 19. Changes (% control) in tumor volumes and ^{31}P intensities of osteosarcoma in mouse #3 during untreated growth.

tumors increased by 70-90% in the period between 0 and 15 days. The increase was 40-70% during days 15 and 25. Changes in PCr, the NTP and Pi resonances are correlated with tumor volumes during growth. Large decreases (40-70%) in PCr and the NTP resonances were found during the first two weeks of untreated growth. Much smaller changes (0-20%) were observed between days 15 and 25. The Pi resonance tended to decrease in the early growth stage and then rapidly increased at the later stage of growth. The PME resonance showed an almost identical pattern as Pi resonance. The tumor pHi (~ 7.1) showed almost no changes at the early stage of growth and then showed a significant drop (~ 6.7) at the very late stages of the growth in most of the mice.

Discussion

The changes observed in untreated growth can be attributed to several major causes: On day 0, we are seeing the spectrum of healthy muscle tissue. As the tumor grows, the spectrum becomes increasingly that of osteosarcoma. As the tumor further grows, the spectrum becomes a mixture of tumor and necrotic tissue. The significant decrease in PCr/Pi is an indication of an increase in tumor/muscle fraction and a decrease in the energy level of the tumors as they became more and more metabolically inactive. The dramatic drop in ATP is believed to be due to a decrease in tumor vascularization between days 0 and 7 (maybe earlier) and an increase in the hypoxic fraction of the tumor. Before inoculation

with tumor cells, the muscle tissue is aerobic and is producing ATP by oxidative phosphorylation, a process in which ATP is formed by adding a phosphate group to ADP. Under aerobic conditions this is responsible for ~ 90% of production of ATP in tissue. Lack of oxygen forces the tumor to generate ATP by glycolysis, a process that is anaerobic and much less efficient. The creatine kinase reaction, also an anaerobic process, becomes more active to maintain the level of ATP. This can also account for the rapid drop in PCr resonance. The decrease in pHi can be attributed to the accumulation of lactic acid, which is an end-product of glycolysis.

At late stages of growth, only the Pi and PME resonances dominate the spectra. This is an indication of increase of dead cells or necrosis. The presence of PCr resonance even at late stages of growth suggested three possibilities: (1) contamination from normal tissues adjacent to the tumor due to insufficient selectivity in NMR signal sampling, (2) signals originated from normal cells that infiltrated the tumor and could not be eliminated with this technique (i.e., tumor heterogeneity), and (3) signals originated from tumor cells which had been shown in previous studies to have the ability to generate PCr of a detectable level by some degree of creatine kinase reaction.

Conclusion

This study demonstrated that ^{31}P MRS from tumors of less than 1 cc in size can easily be detected. With better S/N ratio

(larger number of averages) and a more homogeneous RF coil (such as solenoidal coil), ^{31}P MRS can be a very useful monitor to provide noninvasive information on tumor growth and response to chemotherapy.

NMR studies of tumors are still in their initial stage. Current data obtained by other researchers are largely anecdotal. Definitive conclusions with respect to the potential clinical and experimental utility of this method will require detailed attention to the effects of therapeutic dose, mode of administration, tumor site, and anesthetic agent. The extent of correlation of spectroscopic changes with reliable indices of viability and oxygenation will have to be evaluated. Spectroscopic studies need to be extended to nuclei other than ^{31}P, and assignments of spectral resonances need to be obtained for each tumor. Efficient spatial localization techniques have to be implemented. Proton imaging is needed to assess tumor size and heterogeneity better. Particularly noteworthy is the absence of any study of the kinetics of tumor metabolism by saturation-transfer and other NMR techniques which may lead to the understanding of the dynamic characteristics of tumors.

In Vivo ^{31}P MRS of Cat-Brain Hypoxia

Introduction

Representing only 2% of the total body weight, the human brain has 5-6 times higher metabolic rate than the rest of the body.

The brain consumes 20% of the oxygen and 25% of the glucose used by the body, although brain tissue has a relatively low capillary density with essentially no oxygen stores and comparatively lower concentrations of high-energy phosphate compounds, such as phosphocreatine (PCr). Thus, the normal functioning of brain cells relies, to a unique extent, on a sufficient and continuous supply of oxygen. Even moderate reductions in the rate of delivery can lead to symptoms [42]. Severe reduction can cause irreversible neurologic injury within relatively short periods of time [42]. "Oxygen availability" is defined as the amount of oxygen that is presented to the tissue at any given moment. It is proportional to the product of cerebral blood flow (CBF) and the total oxygen content of arterial blood ($[O_2]_a$), which is determined by the percentage saturation of hemoglobin (SO_2) and by the hemoglobin concentration ([Hb]), thus

$$O_2 \text{ availability} = CBF \bullet SO_2 \bullet [Hb]$$

Hypoxia is defined as a reduction in available oxygen to levels below what are sufficient to maintain normal function, metabolism, or structure. It can be induced by reduction in any one of the three terms that appear on the right-hand side of the above equation. In this experiment, we are interested in "hypoxic hypoxia" which is a reduction in SO_2 and $[O_2]_a$ due to a fall in arterial oxygen pressure (pO_2).

In clinical medicine, hypoxic hypoxia is not common, but occurs in anesthesiological accidents, critically ill patients, as well as in lung disease. It is also encountered at high altitude. Electroencephalography (EEG), a device for monitoring electrical activity generated by brain cells in terms of frequency, has been used clinically to detect certain abnormalities in the brain such as tumors, trauma, and infectious diseases. With progressive reduction in oxygen availability, there is, initially, no change in the EEG [42]. As hypoxia becomes more marked, there are changes in EEG that include a gradual loss of high frequency activity and increase in low frequency activity. With more severe hypoxic stress (<10% O_2), total EEG activity decreases and finally ceases. Changes in the EEG activity have been correlated to changes in oxygen availability. However, the correlation between changes in oxygen availability and energy availability, which can be evaluated as a function of the quantitation of cerebral phosphorus metabolites (ATP, PCr, Pi), has only just begun to be studied. ^{31}P MRS has potential clinical value for evaluation of brain energy state in vivo [43]. The value of ^{31}P MRS is that measurements can be made noninvasively and repeatedly, allowing the comparison of each subject with his own control state. Although changes in the ^{31}P MRS spectra have been reported previously during hypoxic hypoxia and ischemia (fall in CBF), many of them had been done ex-vivo. It is uncertain the extent to which biochemical sampling techniques, such as freezing clamping and high pH extraction, may alter cerebral metabolite concentrations. These ex vivo changes can

relate to neuronal damage and neurologic outcome. The purpose of this in vivo study is to test the sensitivity of ^{31}P MRS at 2T to the cerebral metabolic responses in hypoxic hypoxia, to identify ^{31}P MRS spectral changes which occur during hypoxia, and to relate these changes to neurologic outcome and to histopathology.

Methods and Procedures

Both male and female 3-5 kg colony-bred cats were used in these experiments. A chronic arterial catheter with a subcutaneous access port (Norton port) was inserted into the femoral artery of each cat under isoflurane anesthesia at least one week before the start of the experiment. On the day of the study, the cats were anesthetized, intubated, and ventilated with isoflurane in oxygen. Scalp hair was clipped and Ag/AgCl cup electrodes were attached to with collodion for EEG recording. These EEG electrodes were placed symmetrically on top of the head, equivalent to the International 10-20 system for humans. Simultaneous differential and referential recordings were made using a Nicolet lA97 EEG recorder, and signals were stored on a Vetter FM tape recorder. Standard EEG equipment including silver-plated cups and shielded coaxial cables were used. To isolate EEG signals (1-60 Hz) from RF signals (34-86 MHz), a high-frequency, 25 dB LC filter was applied before EEG signals were fed into the recorder. Lateralized chest leads were used to detect ECG (electrocardiogram, a reading of

electrical changes that accompany the cardiac cycle) signal, and a fiberoptic rectal temperature probe was inserted for physiological monitoring. After centering the cat in the magnet, vercuronium was given for muscle relaxation and isoflurane was withdrawn. For centering in the magnet, the cat was placed in the plexiglass tube and the head was positioned with Teflon ear bars.

After the cat had been on vercuronium for 1 hr and ventilated with 100% O_2, baseline T_2-weighted 10-slice ^1H spin-echo images and three ISIS-localized ^{31}P spectra were obtained. These data established the baseline or control state of the brain. Then hypoxia was induced with inspired O_2 concentration reduced to 8%. Constant infusion of sodium bicarbonate was used to balance system pH. To save the heart from failure when a low systolic arterial pressure (<80 mmHg) was observed, the cat was given 15 sec 100% O_2. Such an "oxygen rescue" was given one or more times during the hypoxic period. When arterial pressure fell to 80 mmHg for the second time, hypoxia was reversed by 100% O_2. This resuscitation period lasted for 1 hr, after which the cat was removed from the magnet, vecuronium was withdrawn, and the cat was allowed to wake up. When the cat could walk unassisted, it was returned to its cage.

The cat was allowed to recover for a week, during which period its neurologic function was monitored daily. ^{31}P MRS and ^1H MRI were performed on day 8 with EEG and other physiological monitoring used as in the first experiment. Then under isoflurane anesthesia, the brain was removed and stored in formalin for

neurohistopathological examination. This examination was performed according to standard techniques using axial sections to be able to compare pathology with images obtained from ^{1}H MRI.

We studied two groups of cats. Group I (cats #1, #2, and #3) had oxygen rescues as described. Because acute hypoxia used in group I has a high potential of producing heart failure and complexity caused by different number of O_2 rescue used for each cat, in group II (#4, #5, and #6) 10% O_2 rescues were done at a constant rate (one rescue every 15 minutes) with the rest of the procedure the same as in group I.

The NMR experiment was performed on a 2T SIS Co. model VIS spectrometer. A half-saddle coil double-tuned to ^{1}H and ^{31}P with the trap-circuit (described in Chapter III) was used for ^{1}H imaging and ^{31}P localized spectroscopy. To localize on the cerebrum, we incorporated the hyperbolic secant inversion pulse with the three-dimensional ISIS technique. The half-saddle coil was made from copper tubing (99.9%) of outer diameter 2.5 mm. This double-tuned balance-matched circuit, ^{31}P (34.6 MHz) and ^{1}H (85.5 MHz), was built with both fixed, high-Q chip capacitors (by American Technical Ceramics--ATC 100), variable capacitors (by Johanson Manufacturing Corporation--JMC P/N 5641, 1-30 pf), and low-noise BNC cable (by ITT Pomona Electronics--4964) on a single-sided printed circuit with the other side shielded with copper tape and grounded to the cable. For 5000 μs sinc pulse (bandwidth = 1000 Hz), the radio-frequency power output was +87 dbm. A 2.5 cm sphere of 300 mM Na_2HPO_4 at the coil center was used to

calibrate the ^{31}P hard pulse length. With +100 dbm radio-frequency power output, the 90° ^{31}P pulse was about 160 μs depending on the depth of the center of the selective volume. After positioning the cat in the magnet, a multislice spin-echo sequence of short TR (500 ms), short TE (20 ms), and low spatial resolution (32 x 256) was used. Ten slices with 3 mm slice thickness separated by 4 mm between slices were obtained in less than 1 minute. Based on this scout image, the cat was repositioned to place the brain at the center of the magnet where the homogeneous B_0 field is. A T_2 -weighted baseline image with TR = 2s, TE = 70 ms, 128 x 256 spatial resolution, 8 cm x 8 cm Field of View and 4 averages in axial planes was then acquired. These images were used to compare with images obtained with the same sequence and parameters after hypoxia. They were also needed to calibrate the gradient settings for the desired size and volume and to determine the center of the volume of interest for the ISIS sequence. Same scout images in the sagittal planes are also needed to determine the center of volume accurately.

Markers containing $CuSO_4$ dopped water were sometimes used for better positioning of EEG electrodes on the cat's head. B_0 homogeneity was adjusted by the ^1H signal with nonlocalized single-pulse sequence. The water linewidth after shimming was 50-60 Hz full width at half height. Shimming usually required between 15-20 minutes.

The ISIS experiment is done by using a phase-swept hyperbolic-secant pulse of 5000 μs pulsewidth (bandwidth = 1600

Hz or 46 ppm) for the inversion pulses. The radio-frequency power output for complete inversion within the sensitive volume of the coil was found to be over +100 dbm as verified by measurements on phantoms that had the same coil loading effect, but was smaller than +118 dbm to avoid coil arcing due to exceeding the rated voltages of the components in the tuned circuit. The inversion pulses are followed by 90° nonselective excitation pulse. The frequency of the selective inversion pulse and the gradients used were determined from the T_2-weighted image. Each inversion defines a plane. The intersection of three orthogonal planes defines the cube from which the ^{31}P signals originate. The selective volumes were approximately 6.5 cc and were completely in the cerebrum of the brain. Phase cycling of the 90° excitation pulse and receiver was used. A delay of 20 msec prior to the excitation pulse allowed the residual gradients to decay.

The eight experiments required for the three-dimensional ISIS sequence were obtained separately in blocks of 64 scans with a spectral width of 2000 Hz. Each scan had a repetition rate of 1.5 sec. The purpose of the rapid pulsing was to improve the measurement of pHi by enhancing the prominence of the Pi resonance relative to neighboring phosphomonoester and phosphodiester resonances which were relatively more saturated by reason of their longer T_1's [44, 45]. A delay of 12 sec between experiments allowed for full T_1 relaxation to avoid signals from outside of the volume of interest.

Free induction decays were Fourier transformed with a 10 Hz Lorenzian line broadening, the broad resonance (hump) from relatively immobile phosphates (mainly from bone and phospholipid) was removed by a profiling procedure (convolution difference method) with line broadening of ~ 350 Hz. The peak areas were determined by planimetry.

Results

Figure 20 shows four sequential slices of the T_2-weighted 10-slice image of the cat's brain. The gap between two adjacent slices is ~ 1 mm. Each slice is 3 mm thick with a spatial resolution of 256 (x) x 128 (y) and field of view of 8 cm x 8 cm. The in-plane pixel size is 0.3 x 0.6 mm. The frequency encoding gradient is along the x direction and the phase encoding is along the y direction. Gray matter, white matter, and cerebrospinal fluid of the brain are clearly seen.

Figure 21 shows a typical series of ^{31}P spectra before, during, 1 hour after, and 7 days after hypoxia in group I. In this group of experiments, the decrease in inspired oxygen had immediate effects on blood gases which could be seen in decrease of pO_2. The pHi is determined by the chemical shift difference (ΔPi in ppm) between PCr and Pi resonances using a predetermined titration curve. Because existing NMR titration data on Pi are not fully appropriate for work on brains, a study was done to establish a

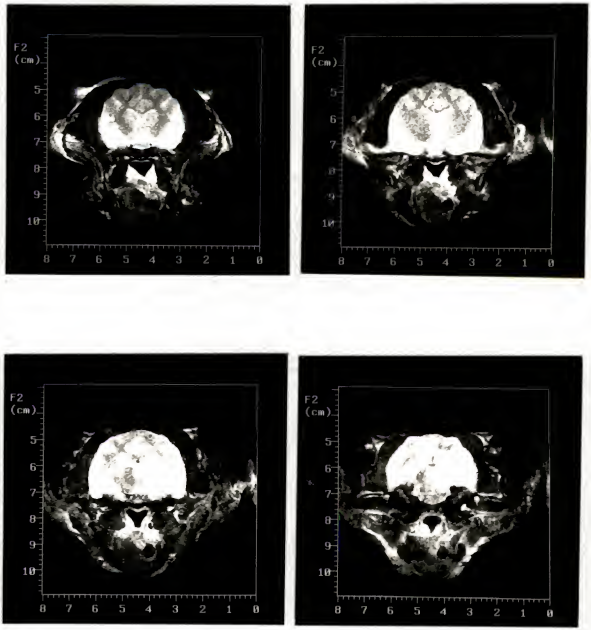

Figure 20. Four consecutive slices of a cat's head using multi-sliced T_2-weighted spin-echo sequence.

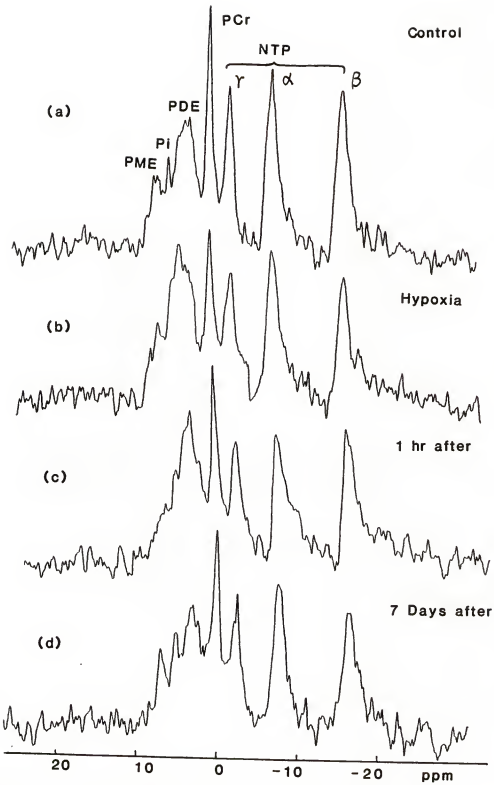

Figure 21. Typical ISIS-localized ^{31}P spectra of cat brain hypoxia in Group I: (a) control, (b) hypoxia, (c) 1 hr after hypoxia, and (d) 7 days after hypoxia.

suitable constant in the Henderson-Hassalbalch equation [46]. This relation

$$pHi = 6.77 + \log [(\Delta Pi - 3.29) / (5.68 - \Delta Pi)]$$

was used in our study.

Figures 22-24 show the time course of phosphorus metabolites and intracellular pH changes during the entire experiment. During the early period of the oxygen changes, the ^{31}P spectra were not significantly different from those obtained under control conditions (100% O_2). Prolongation of the hypoxia resulted in changes in the spectra in 2 cats, #1 and #3, which, a week later, showed a high and medium degree, respectively, of white matter pathology in the cerebrum from a histopathology examination. These changes are up to ~30% decrease of the PCr resonance and up to ~60% increase of the Pi resonance. This, therefore, gives a decrease in PCr/Pi ratio up to ~ 70%. A decrease in the intracellular acidification, pHi in Table 5, was also observed. Despite the biochemical fact that the rate of ATP consumption or production is buffered by the conversion of PCr to ATP via creatine kinase reaction, the β-NTP resonance (containing only ~60% of ATP) and the γ-NTP resonance (containing ~60% ATP and ~6% ADP) showed a decreasing trend during hypoxia and did not recover fully after oxygen resuscitation. However, these changes could not be related to prolongation of hypoxia, concentration of other phosphorous metabolites, pHi or EEG reading in this study.

TABLE 5. SUMMARY OF CHANGES OF ^{31}P METABOLITES AND pHi IN CAT'S BRAIN BEFORE, DURING, AND AFTER HYPOXIA FOR GROUP I CATS[a]

	PC_r	Pi	PCr/Pi	γ-NTP	α-NTP	β-NTP	pHi
CAT #1							
Baseline	10	2.7	3.7	7.4	8.8	8.3	7.01
Hypoxia[b]	7.6	3.3	2.3	6.7	8.3	8.0	6.87
Posthypoxia[c]	9.4	2.9	3.3	6.5	8.9	8.3	6.89
Follow-up[d,e]	9.1,	5.9,	1.5,	6.1,	11.4,	8.8,	7.13,
	9.1	4.4	2.1	6.7	11.5	8.9	7.04
CAT #2							
Baseline[e]	9.8,	2.9,	3.4,	8.6,	12.1,	9.6,	7.17,
	9.6	2.9	3.3	8.5	12.7	9.6	7.20
Hypoxia[b]	9.3	3.2	2.9	9.1	12.9	9.5	7.07
Posthypoxia[c]	9.3	2.5	3.7	8.0	11.1	8.8	7.16
Follow-up[d,e]	9.3,	4.4,	2.1,	8.2,	12.1,	9.6,	7.06,
	9.3,	4.8,	2.0,	8.4,	12.3,	9.8,	7.13,
	9.1,	4.5,	2.0,	8.4,	11.6,	9.6,	7.05,
	9.1	4.5	2.0	8.4	11.6	9.8	7.05
Cat #3							
Baseline	10	2.8	3.6	8.4	12.6	11.6	7.09
Hypoxia[b]	7.0	5.4	1.3	6.6	10.8	9.2	6.24
Posthypoxia[c]	8.0	2.8	2.9	6.2	8.6	9.2	7.03
Follow-up[d,e]	9.2,	4.0,	2.3,	9.0,	11.2,	9.4,	7.07,
	11.0,	4.0,	2.8,	8.4,	11.6,	10.2,	7.11,
	11.6	3.6	3.2	8.8	10.4	10.2	7.08

[a]All values are normalized to the highest PCr peak (10) in every cat.
[b]"Hypoxia" values were taken from the spectrum which had the lowest PCr/Pi.
[c]"Posthypoxia" values were taken from the spectrum obtained 1 hour after O_2 resuscitation.
[d]"Follow'up" values were taken from the spectra obtained 1 week after hypoxia.
[e]Numbers separated by a comma are values from each of the 2-4 spectra.

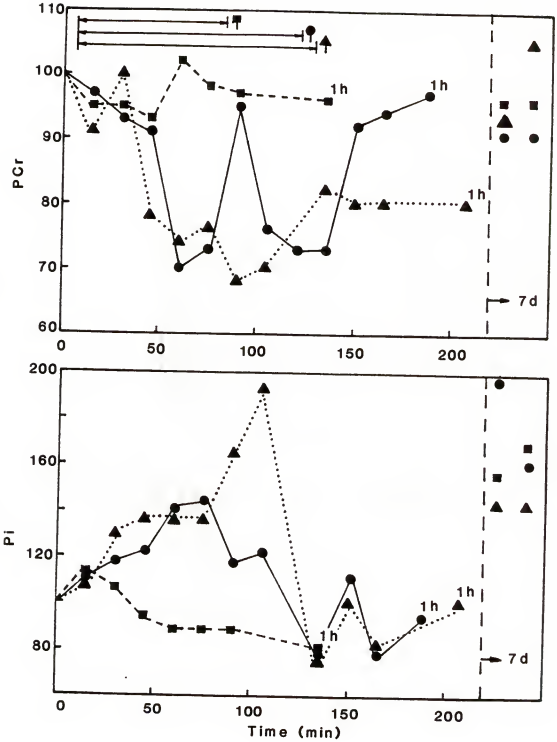

Figure 22. Time course plot of the changes (% control) PCr and Pi of cat brain hypoxia in Group I. (circle: cat #1, square: cat #2, triangle: cat #3, 1 h = 1 hour after hypoxia and _____: hypoxic period)

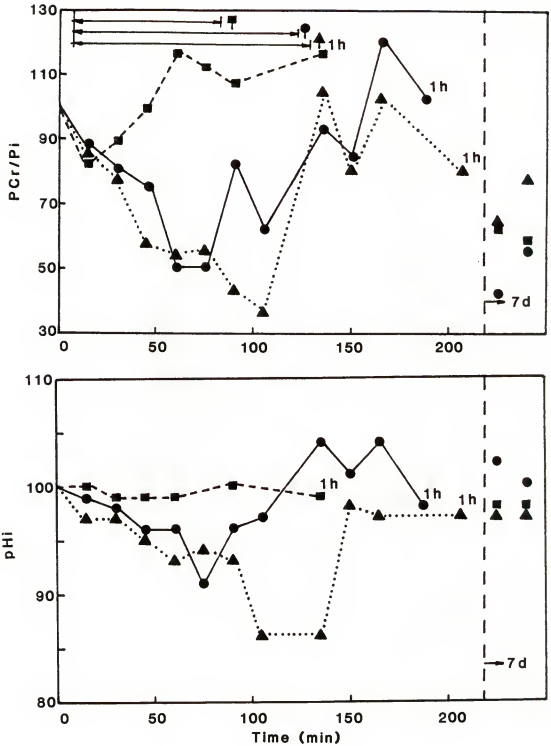

Figure 23. Time course plot of the changes (% control) in PCr/Pi and pHi of cat brain hypoxia in Group I. (circle: cat #1, square: cat #2, triangle: cat #3, 1 h: 1 hour after hypoxia and ____: hypoxic period)

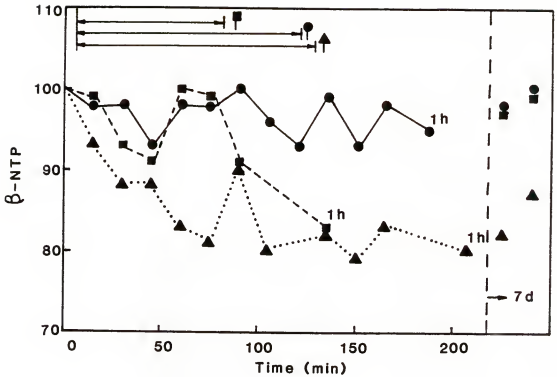

Figure 24. Time course plot of the changes (% control) in β-NTP of cat brain hypoxia in Group I. (circle: cat #1, square: cat #2, triangle: cat #3, 1 h: 1 hour after hypoxia and ____: hypoxic period.

Cat #2, which showed no pathology at all a week later showed much smaller changes in the spectra with small changes in PCr resonance, no changes in ΔPi and even a decrease in Pi resonance 1 hour after hypoxia. During 100% O_2 resuscitation, peak intensities and pHi changed in a reverse manner than during hypoxia. PCr/Pi ratio returned to nearly control value 1 hour after resuscitation. Follow-up spectra, 7 days after hypoxia, showed elevated Pi resonances in all three cats. Nearly "control" level of PCr and ΔPi were clearly observed in all three cats in group I. No significant changes in PME and PDE were found during the entire experiment. EEG scores during hypoxia showed perfect rank order with pathological scores.

Figure 25 shows a typical series of ^{31}P spectra before, during and 1 hour after hypoxia for the group II cat study which had periodic O_2 rescue as described above. A similar pattern of spectral changes were observed for group I. However, the changes are much smaller, especially for pHi (see Table 6). Figures 26-28 show the time course of phosphorus metabolite levels and pHi during the entire experiment of this group. Our data also show that cerebral pHi was more effectively regulated than the pH of the arterial blood which was periodically measured at the end of acquisition of each spectra. This can be due to the combination of causes, such as the use of sodium bicarbonate and the fact that regulation of pHi by living systems is the net result of several interacting processes.

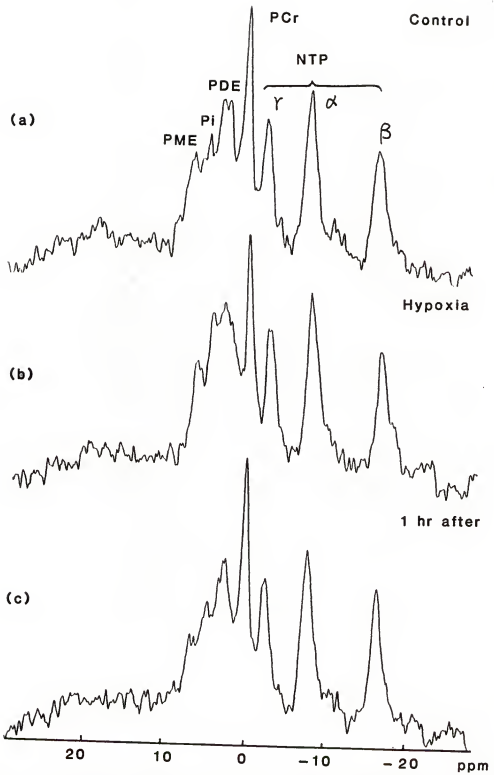

Figure 25. Typical ISIS-localized ^{31}P spectra of cat hypoxia in Group II: (a) control, (b) hypoxia, and (c) 1 hr after hypoxia.

TABLE 6. SUMMARY OF CHANGES OF ^{31}P METABOLITES AND pHi IN CAT'S BRAIN BEFORE, DURING, AND AFTER HYPOXIA FOR GROUP II CATS[a]

	PC_r	Pi	PCr/Pi	γ-NTP	α-NTP	β-NTP	pHi
CAT #4							
Baseline[b]	10.0,	3.4,	3.0,	7.2,	10.2,	7.5,	7.04
	9.9,	3.2,	3.1,	7.3,	9.7,	8.2,	7.05
	9.4	3.5	2.7	7.2	10.4	7.3	7.00
Hypoxia[c]	8.5	3.5	2.5	7.4	10.2	7.5	7.01
Posthypoxia[d]	9.3	3.1	3.0	6.9	9.4	17.0	7.01
CAT #5							
Baseline[b]	9.6,	2.9,	3.3,	7.8,	11.0,	7.9,	6.96
	10.0,	2.9,	3.4,	7.5,	10.1,	8.0,	6.97,
	9.7	2.8	3.5	7.8	10.4	8.0	6.97
Hypoxia[c]	8.7	4.4	2.0	7.3	10.9	8.1	6.78
Posthypoxia[d]	9.5	3.4	2.8	7.2	10.9	8.0	6.90
Cat #6							
Baseline[b]	10.0,	3.2,	3.1,	7.2,	9.8,	7.4,	7.26,
	9.3,	3.3,	2.8,	7.4,	10.1,	7.1,	7.21,
	9.2,	3.4,	2.7	6.9,	9.7,	7.7,	6.98,
	10.0	3.4	2.9	7.3	10.1	7.0	7.09
Hypoxia[c]	8.3	4.1	2.0	7.8	9.6	7.3	7.15
Posthypoxia[d]	9.0	3.1	2.9	7.0	9.5	6.6	7.06

[a]All values are normalized at highest PCr peak (10) in every cat.
[b]Numbers separated by a comma are values from each of the 3-4 spectra.
[c]"Hypoxia" values were taken from the spectrum which had the lowest PCr/Pi value.
[d]"Posthypoxia" values were taken from spectrum obtained 1 hour after O_2 resuscitation.

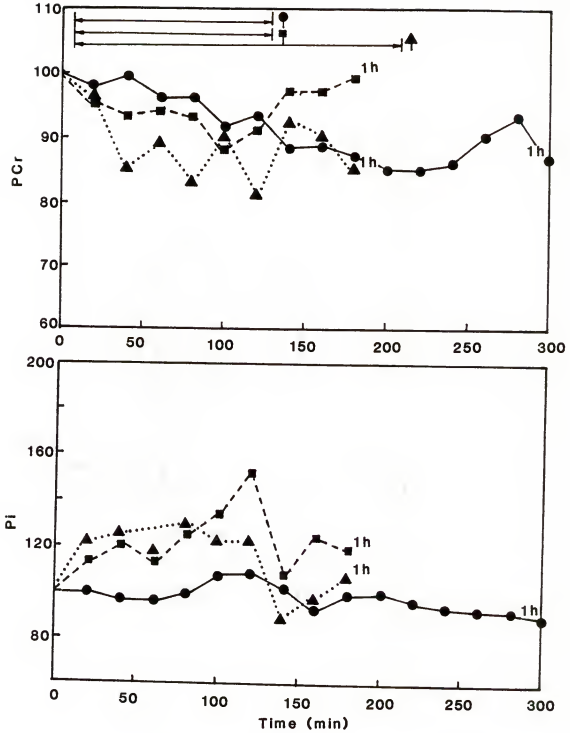

Figure 26. Time course plot of the changes (% control) in PCr and Pi of cat brain hypoxia in Group II. (circle: cat #4, square: cat #5, triangle: cat #6, 1 h: 1 hour after hypoxia and ____: hypoxic period)

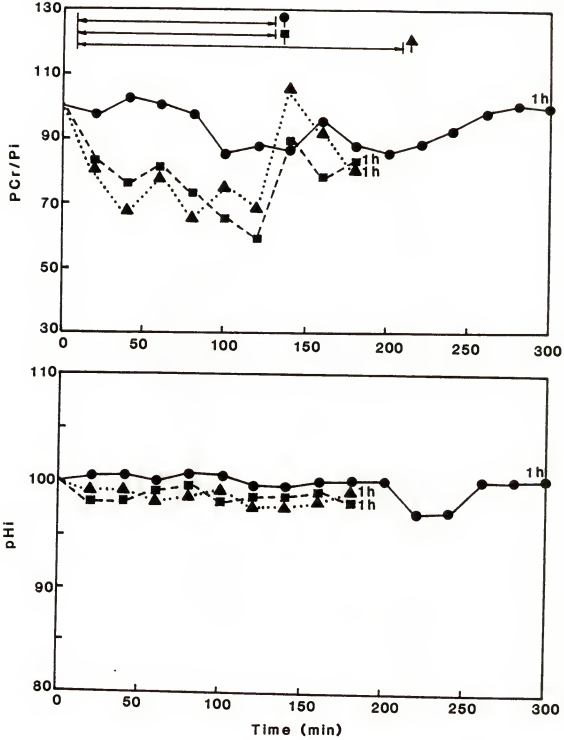

Figure 27. Time course plot of the changes (% control) in PCr/Pi and pHi of cat brain hypoxia in Group II. (circle: cat #4, square: cat #5, triangle: cat #6, 1 h: 1 hour after hypoxia and ____: hypoxic period)

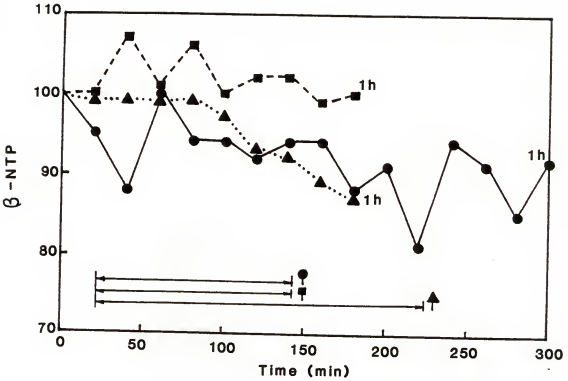

Figure 28. Time course plot of the change (% control) in β-NTP of cat brain hypoxia in Group II. (circle: cat #4, square: cat #5, triangle: cat #6, 1 h: 1 hour after hypoxia and ____: hypoxic period)

Discussion

Our data demonstrate that ^{31}P MRS at 2T is sensitive to cerebral metabolic responses to external changes such as hypoxic hypoxia. Phosphorus MRS provides vital information about changes in ^{31}P metabolite levels that was available previously only by invasive methods. In general, our findings agree well with those of previous workers who used biochemical techniques to study the metabolic effects of hypoxic hypoxia. These studies showed that the change in the cerebral oxygen supply is accompanied by changes in the quantities of energy-rich phosphates, and the extent of the change is related to the duration of hypoxia. In this study, we found no reason to suspect that ^{31}P MRS measurements made in vivo with a surface coil using ISIS sequence are subject to unanticipated artifacts or distortions. It is therefore appropriate to assess the metabolic significance of our observations, which in some instances go beyond earlier biochemical data. Because of the chemical shift displacement effect, the fractional tissue components effects, as well as not fully relaxed spectra, resonances from different metabolites cannot be compared with one another. But peak intensity changes of one particular resonance can certainly reflect concentration change at different stages of the hypoxia accurately. Therefore, plotting data as % control vs. time is perhaps the best way to present data in a time course study such as this.

A problem often encountered in brain studies is that resonances of relatively narrow linewidths are superimposed on a

rather broad component due to bone and other immobile molecular species such as phospholipid. This affects accurate metabolite quantitation obtained by integrating the area under each resonance peak. The problem can be solved by using a convolution difference technique. It is assumed that the broad line is Loretzian in shape with a T_2 much smaller than any of the narrow resonances of interest without distorting peak heights, areas and ΔPi.

However, a more annoying problem is the severe overlapping of a group of resonance peaks (PDE, Pi, and PME) between 2 to 6.5 ppm on the downfield side of PCr. This is due to inherently broad signals from the PDE-containing phospholipids (found in high concentrations in nerve and brain tissue) in the region around 2.5 ppm and the small chemical shifts among these peaks. The PDE peak consists of two resonances: one resonance GPC or glycerol 3-phosphorylcholine, at 1.5-2 ppm, and the other GPE or glycerol 3-phosphorylethanolamine, at 2.5-3 ppm. In the case of Pi, the peak was at around 5 ppm. The PME peak consists of two resonances, one resonance PC, phosphorylcholine, at 6-6.5 ppm, the other resonance at 6.5-7 ppm. The lack of spectral resolution can severely affect the accuracy of peak area measurements. This effect can bury the Pi resonance under the PDE resonance, especially during the hypoxic process when acidity of the brain tissue increases and the Pi peak moves toward PDE peak. This makes pHi difficult to determine. To get around this problem, previous studies [47] had suggested the use of the chemical shift difference between γ-ATP and α-ATP (Δ ATP) to calculate pHi by using pH

titration curves obtained by varying the concentration of Mg^{+2} in the solution. We had fit our in vivo data (Δ ATP in ppm drawn from the ^{31}P spectra) to the following equation for 2.5 mM Mg^{+2}, which is comparable to the physiological level found in the brain:

$$pHi = pK + \log [(\Delta ATP - \delta^{+}) / (\delta^{-} - \Delta ATP)]$$

where pK = 5.776, δ^{+} = 0.537, and δ^{-} = 5.481. We found no relation whatsoever between these results and those we obtained by using chemical shift differences between Pi and PCr resonances (ΔPi) which can be related to ^{31}P metabolites and EEG changes. This result does not imply the uselessness of the ΔADP approach under this condition but the complexity of it, namely the effect of Mg^{+2} concentrations on ATP phosphates. The effects of increased Mg^{+2} concentration are (1) line broadening effects as manifested by a loss of peak multiplicty and a decrease of peak amplitude, (2) a decrease of homonuclear phosphorus coupling constants, and (3) a decrease of pK values in the above equation. A detailed study of these effects can not only lead to accurate measurement of pHi but also the estimation of intracellular Mg^{+2} concentration.

We also found in calculating pHi using ΔPi that the use of different titration curves (different calibration parameters) did make a difference in absolute pHi while fractional change (or percentage change), which we report in this study, did not. This is not so surprising when only the linear portion of a titration curve is used.

Further improvements in the NMR aspect of the experiment can be done by the following:

(1) The use of a shorter pulsewidth but well-behaved hyperbolic-secant inversion pulse can not only provide a wider frequency range for more uniform excitation, but can also reduce the chemical shift displacement to slice thickness ratio by using higher gradient strength for the same voxel size.

(2) The chemical shift displacement can be eliminated by combining a specially designed pulse sequence suggested by Hall [32], with the ISIS sequence.

(3) Spectral resolution and S/N can be greatly improved by doing ^{1}H-decoupling and ^{31}P-decoupling simultaneously [48].

(4) Adopting a reliable spectral fitting routine will be extremely helpful in determining the peak area of each resonance with consistency and accuracy, especially when overlapping of peaks is severe.

(5) The use of a higher field magnet (> 2 Tesla) would be extremely useful. This would allow achieving better S/N ratio within the same scan time for static studies and would allow shorter scan time for the same S/N ratio in a time course study. Shorter spectral accumulation time in time course studies would avoid averaging effect, which can mask physiological response. A higher field magnet will also increase spectral resolution (frequency separation among peaks in a spectrum), which will reduce peak overlapping and improve the accuracy of the peak area determination.

Significance

We have adopted existing knowledge to develop the NMR portion of the cat hypoxia study. We have also found that the PC_r/P_i ratio seems to be of use both for assessment of tissue damage and for prediction of neurologic outcome after metabolic stress. Even though we are still evaluating and further exploring the biological models (Model I or Model II), the NMR portion of the study is sufficiently well developed that these biological models can now be fully explored.

CHAPTER VI
SIGNIFICANCE AND CONCLUSIONS

The significance and conclusions of the whole research can be summarized as follows:

1. A method to obtain absolute metabolite molar concentrations of ^{31}P or other nuclides has been developed, optimized, and used. This method uses tissue water concentration as an internal standard. Because of the frequency dependence of the RF penetration depth, this method is most suited for the study of small animal modles (such as mice and rats) or superficial tissues in humans. This method can be used in conjunction with either a surface coil or a volume coil as long as the effective penetration depth is much larger than the dimension of the sensitive volume. In vivo data from normal mouse gluteus muscle have shown good agreement with values previously obtained by others using biochemical analysis. We suggest that reference to ^{2}H (in HDO) rather than to ^{1}H may give better accuracy and more flexibility in the quantitation results.

2. A method to obtain absolute metabolite molar concentrations using the same nuclide as an external reference has been developed, optimized, and used. This method avoids the complexity and tediousness of obtaining the B_1 profile of a coil and

of compensating for different sample loading effects. In conjunction with localization techniques, this method can be used for deep-seated tissues because of the same RF penetration depth for the same nuclide. This method can be applied to a surface coil or a volume coil. Using this method, in vivo data from the cat's brain have shown good agreement with values reported previously.

3. A review of existing localization methods, both B_0-gradient methods (Table 2) and B_1-gradient methods (Table 3) has been conducted. The comparison among these methods should serve as a good starting point when a localization method is desired for a specific experiment. This review can also be used as a reference when one tries to characterize a newly developed method.

4. The accuracy of the ISIS sequence for localization and its use in conjunction with the hyperbolic-secant pulse to optimize S/N of a spectrum have been demonstrated. This sequence has been implemented successfully in the cat brain hypoxia study. Because of its flexibility of changing the size of the localized volumes, flexibility of moving the volume in space, non-T_2-weighted nature of the NMR signal, ability to be applied to coils that show gross B_1 inhomogeneity, and ability to extend to multiple and conformal volumes, the ISIS sequence should find wide applications in human and large animal models.

5. Slice thickness-gradient relation curves have been experiementally determined for ^{31}P and ^{1}H using the hyperbolic-secant pulse on the 2T VIS imager/spectrometer. These curves will be very useful for future users of this machine.

6. The chemical shift displacement effect, which occurs when localization is achieved by slice selection in the presence of many chemically shifted species, was assessed. The use of a selective pulse of wider bandwidth (shorter pulse duration) in conjunction with a stronger gradient to reduce the chemical shift effect is recommended.

7. The effect of T_1 relaxation on localization was evaluated. We found that when a coil with inhomogeneous B_1 field is used, care should be taken, because the relaxation affects the accuracy of localization when metabolites of different T_1's are present.

8. Several conclusions that we drew in regard to localized shimming, described in Chapter III, can be used as a guideline when short shimming time but good B_0 homogeneity is desired for an experiment.

9. A mathematical model designed to separate contributions from different tissue components in a spectrum obtained from a VOI has been proposed. In conjunction with MRI to differentiate different tissue components within an image, this method may be shown to be a tool to improve localization of heterogeneous tissues.

10. A systematic examination of the characteristics and comparison of the performance of three different double-tuned coil designs have been conducted. The trap-circuit design has been chosen for use for in vivo studies in this research. This design has some obvious advantages over the other two designs described in Chapter IV. Its wide applications for in vivo study are expected.

11. The conclusions we drew in Chapter IV in regard to coil performance can be used as a guideline when comparing different coil designs.

12. The mouse tumor study has demonstrated that ^{31}P MRS from tumors of less than 1 cc in size can be easily detected. Phosphorus metabolite concentrations have been found to be related to tumor growth. This will aid our understanding of tumor growth and to what extent in vivo spectroscopy can follow tumor growth. Studies of this kind should prove to be useful monitors to evaluate response to cancer treatment.

13. We developed the NMR portion, localization and quantitation, of the cat brain hypoxia project. This study has demonstrated that ^{31}P MRS can be correlated with neurological changes following brain hypoxia in cats. Since our long-range goal is to minimize hypoxic brain injury in patients during anesthesia or critical illness, these results would be very helpful for patient management. Even though we are still evaluating and further exploring other biological models of feline brain hypoxia, the NMR portion of the study is sufficiently well developed that these biological models can now be fully explored.

In summary, this research has developed and perfected techniques for the localization and quantitation of ^{31}P spectra in vivo. The methods have been tested on the mouse tumor and cat brain hypoxia models. However, the experience gained in this research can be applied directly to other biological experiments on

the 2T VIS spectrometer. Moreover, the results should be able to be extrapolated to other spectrometer systems.

APPENDIX A
DUAL-GAUGE TECHNIQUE FOR COMPUTER TOMOGRAPHY

The attenuation of a beam of photons incident on an absorber of thickness ΔX is descried by the following exponential equation:

$$I = I_o \exp(-\mu \bullet \Delta X) \qquad [1]$$

where I is the incident photon intensity, I_o is the transmitted photon intensity, and μ is the linear attenuation coefficient which is dependent upon the photon energy and physical properties, namely, density and effective atomic number, of the absorber. In the case of X-ray transmitted computer tomography (CT), an image is reconstructed by displaying μ as a function of space within a slice in a two-dimensional case using the Fourier method. However, the error due to composition variation, mainly variation in atomic numbers, of the sample is not accounted for.

To reduce this error and gain more information about the variation of composition in space within the sample, a dual-gauge technique based on phenomenological model can be used. Such model is given by

$$R = f(\rho, g(z)) \qquad [2]$$

where R is the detector response, ρ is the density, g(z) is a function of atomic number (or composition), and f is the function that causes the relation to be a definition. The applicability of equation [2] can be demonstrated by fitting data from a sample of known density and composition by least square method and taking advantage of the fact that the response of two gauges have different relative sensitivities (interaction cross section) to different photon-matter interaction mechanisms, such as Compton, photoelectric, pair production effects, i.e.,

$$R_1 = f_1(\rho, g(z)) \qquad [3]$$

$$R_2 = f_2(\rho, g(z)) \qquad [4]$$

where subscripts 1 and 2 are for two different detectors.

One can solve equations [3] and [4] simultaneously for ρ and g(z), which vary as a function of space within the sample. Better contrast may be achieved by displaying ρ and g(z) separately instead of μ only. A preliminary scanning system using this technique is recommended as in Figure 29.

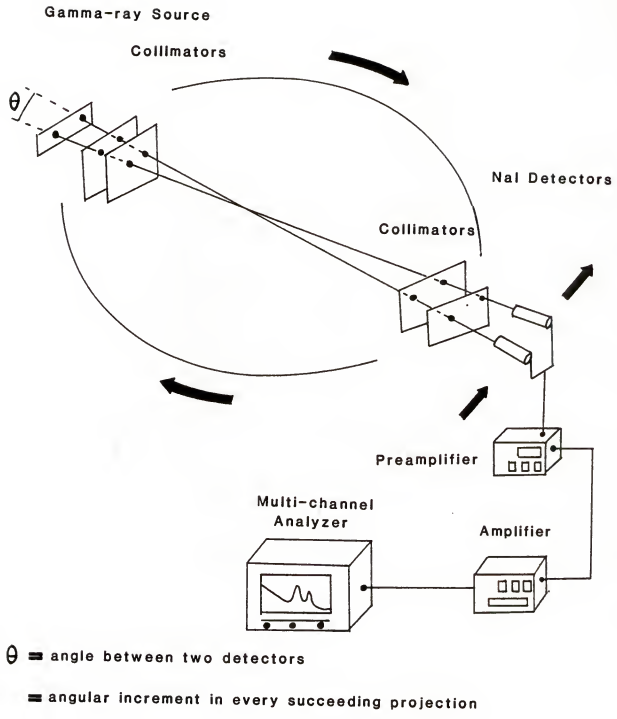

Figure 29. A preliminary scanning system design for CT using dual-gauge principle.

APPENDIX B
QUANTITATION METHOD FOR ABSOLUTE MOLAR CONCENTRATIONS

The relationship between the magnitude of the induced emf (electromotive force) in an NMR experiment and the strength of the B_1 field generated at the sample in the RF coil can be described by equation [1] if the sample of volume V is situated in a region of homogeneous B_1 field.

$$emf = k \bullet B_1 \bullet \sin(\theta) \bullet C \bullet V \qquad [1]$$

where k is a nuclear-dependent constant, B_1 is the B_1 field strength, θ is the tip angle, and C is the absolute molar concentration.

However, B_1, and therefore θ which is proportional to integration of B_1 w.r.t. time, is usually inhomogeneous within the sensitive volume of an RF coil due to either the geometry or construction of it. Therefore, equation [1] needs to be modified as in equation [2].

$$emf = k \int_V B_1 \bullet \sin(\theta) \bullet C \bullet dV \qquad [2]$$

where B_1, θ and C are all functions of space (for example, x, y, z in the case of Cartesian coordinate).

For a multiple-tuned coil, tuned for nuclide 1, 2, 3, ---, it will produce the same spatial distribution of B_1 for all nuclides assuming the penetration effect, which is a function of resonance frequency, is negligible. The ratio of emf's for nuclides 1 and 2, in the case of a double-tuned coil, is given by

$$\frac{emf_1}{emf_2} = \frac{k_1 \cdot C_1}{k_2 \cdot C_2} = K\frac{C_1}{C_2} \qquad [3]$$

where K is the ratio of k_1 to k_2 provide that

(a) both nuclides have the same sensitive volume,

(b) both nuclides either see the same B_1 profile or they are proportional everywhere in space,

(c) tip angles are adjusted such that they are the same for both nuclides at one spatial point, then, everywhere in space,

(d) both nuclides have uniform distribution in concentration within sensitive volume.

A calibration curve, then, can be drawn to relate the ratio of signal intensities (or peak areas) to the ratio of nuclide concentration by matching the tip angle of both frequencies at a position within the sensitive volume of the coil. Absolute molar concentration of one nuclide can be determined if that of the other is known.

REFERENCES

1. G. N. Hounsfield, British J. Radiology, 46, 1016 (1973).

2. W. Kuan and W. Mauderli, Annual Research Review Meeting, Department of Radiology, University of Florida (1987).

3. P. A. Bottomley and C. J. Hardy, Soc. Magn. Reson. Med. 7th Annual Meeting, San Francisco, p. 824 (1988).

4. K. Roth, B. Hubesch, S. Naruse, J. Gober, T. Lawry, M. Boska, G. Matson, and M. Weiner, Soc. Magn. Reson. Med. 6th Annual Meeting, New York, p.608 (1987).

5. D. Hawkes, C. Barton, L. Rodringues, M. Jenkins, and J. Griffiths, Soc. Magn. Reson. Med., 4th Annual Meeting, London (1985).

6. N. R. Shine, J. A. Xuan, A. P. Koretsky, and M. W. Weiner, Magn. Reson. Med. 4, 244 (1987).

7. K. R. Thulborn and J. J. H. Ackearman, J. Magn. Reson. 55, 357 (1983).

8. J. P. Idstrom, Am. J. Physiol. 10, 248 (1985).

9. P. Roschmann, Med. Physics 14(6), 922 (1987).

10. M. D. Schnall, V. H. Subramanian, J. S. Leigh, Jr., and B. Chance, J. Magn. Reson. 65, 122 (1985).

11. R. J. Ordidge, A. Connelly, and J. A. B. Lohman, J. Magn. Reson. 66, 283 (1986).

12. P. N. Venkatasubramanian, M. Barany, I. M. Siegel, A. C. Wilbur, G. S. Zwicky, and P. T. Heydemann, Soc. Magn. Reson. Med. 7th Annual Meeting, San Francisco, p. 823 (1988).

13. J. Vermeulen, P. R. Luyten, and J. A. Hollander, Soc. Magn. Reson. Med. 6th Annual Meeting, New York, p. 136 (1987).

14. L. D. Hall, V. Rajanayagam, and S. Sukumar, J. Magn. Reson. 51, 147 (1983).

15. K. N. Scott, H. R. Brooker, J. R. Fitzsimmons, H. F. Bennett, and R. C. Mick, J. Magn. Reson, 50, 339 (1982), and reference cited.

16. W. P. Aue, Rew. Magn. Reson. Med. 1, 21 (1986).

17. W. P. Aue, S. Mueller, T. A. Cross, and J. Seeling, J. Magn. Reson. 56,350 (1984).

18. P. R. Luyten and J. A. den Hollander, Magn. Reson. Imag. 20, 131 (1986).

19. R. J. Ordidge, M. R. Bendall, R.E. Gordon, and A. Conelly, Magn. Reson. in Biology and Medicine, Tata McGraw-Hill, New Delhi (1985).

20. A. J. Shaka and R. Freeman, J. Magn. Reson. 59, 169 (1984).

21. J. J. H. Ackerman, T. H. Grove, G. G. Wong, D. G. Gadian, and G. K. Radda, Nature 283, 167 (1980).

22. M. R. Bendall and R. E. Gordon, J. Magn. Reson. 58, 365 (1983).

23. R. Tycko and A. Pines, J. Magn. Reson.60, 156 (1984).

24. K. R. Metz and R. W. Briggs, J. Magn. Reson. 64, 172 (1985).

25. P. A. Bottomley, T. B. Foster, and R. D. Darraow, J. Magn. Reson. 59, 338 (1984).

26. J. Vermeulen, P. R. Luyten, and J. A. Hollander, Soc. Magn. Reson. Med. 6th Annual Meeting, New York, p. 136 (1987).

27. C. Remy, J. P. Albrand, A. L. Benabid, M. Decorps, M. Jacrot, J. Riondel, and M. F. Foray, Magn. Reson. Med. 4, 144 (1987).

28. P. Bottomley, United States Patent N. 4480288 (1984).

29. R. J. Ordidge, Magn. Reson. Med. 5, 93 (1987).

30. R. J. Ordidge, Soc. Magn. Reson. Med. 7th Annual Meeting, San Francisco, p. 751 (1988).

31. J. Sharp and M. O. Leach, Soc. Magn. Reson. Med. 7th Annual Meeting, San Francisco, p. 705 (1988).

32. R. R. Ernest and R. E. Morgan, Mol. Phys. 26, 49 (1973).

33. D. N. Kennedy, IEEE Trans. Med. Imaging, Vol. 8, No. 1, March 1989).

34. V. R. Cross, R. K. Hester, and J. S. Waugh, Rew. Sci. Instrum. 47, 12 (1976).

35. J. F. Martin and C. P. Daily, Magn. Reson. Med. 3, 346 (1986).

36. J. R. Fitzsimmons, H. R. Brooker, and B. Beck, Magn. Reson. Med. 5, 471 (1987).

37. S. S. Rajan, J. P. Wehrle, and J. D. Glickson, J. Magn. Reson. 74, 147 (1987).

38. J. D. Glickson, W. T. Evanochko, T. T. Sakai, and T. C. Ng, NMR Spectroscopy of Cells and Organisms, Vol. 1, R. K. Gupta (Ed.), CRC Press: Boca Raton (1987).

39. B. M. Cullen and H. C. Walker, Int. J. Radia. Biol. 48, 761 (1985).

40. D. E. Bullard, S. C. Schold, S. H. Bigner, and D. D. Bigner, J. Neuropathol. Exp. Neurol. 40, 410 (1981).

41. J. M. Dawson and P. D. Wolkie, Recent Advances in Physio. 10, 247 (1984).

42. F. W. Sharbrough, Stroke 4, 674 (1983).

43. M. Hilberman, V. H. Subramanian, J. Haselgrove, J. B. Cone, J. W. Egan, L. Gyulai, and B. Chance, J. Cereb. Blood Flow Metab. 4, 334 (1982).

44. P. L. Hope, E. B. Cady, and P. S. Tofts, Lancet 2, 366 (1984).

45. J. J. H. Ackerman, J. L. Evolhoch, B. A. Berkowitz, G. M. Kichura, R. K. Deuel, and K. S. Lown, J. Magn. Reson. 56, 318 (1984).

46. O. A. C. Petroff, J. W. Prichard, K. L. Behar, J. R. Alger, J. A. Hollander, and R. G. Shulman, Neurology 35, 781 (1985).

47. J. W. Pettegrew, G. Withers, K. Panchalingam, and J. F. M. Post, Magn. Reson. Imaging 6, 135 (1988).

48. P. R. Luyten, G. Bruntink, A. Heerschap, F. M. Sloff, Soc. Magn. Reson. Med. 6th Annual Meeting, San Francisco, p. 708 (1988).

BIOGRAPHICAL SKETCH

Wei-peng Kuan was born in 1957, Taipei, Taiwan, Republic of China. He received his Bachelor of Nuclear Engineering degree from the National Tsing-Hua University, Taiwan. After finishing compulsory military service, he worked as a nuclear reactor fuel engineer for a nuclear power company. Because of the academic attraction and an offer of a teaching assistantship, he became a graduate student in the Nuclear Engineering Department of the North Carolina State University (NCSU) in 1982, where he received the Master of Nuclear Engineering degree with emphasis on radioisotopes applications in medicine. Because of a strong desire for further research in medical radiation physics and also the high academic standing at the University of Florida, he became a graduate student in the Nuclear Engineering Sciences Department of the University of Florida in 1984. He is presently pursuing the degree of Doctor of Philosophy in medical physics with emphasis on magnetic resonance in vivo spectroscopy and imaging. He is married to a lovely wife, Lee-hui, and has a son, Jonathan, who is one-and-a-half years old.

I certify that I have read this study and that in my opinion it conforms to acceptable standards of scholarly presentation and is fully adequate, in scope and quality, as a dissertation for the degree of Doctor of Philosophy.

K. N. Scott

Katherine N. Scott, Chairman
Professor of Nuclear Engineering Sciences

I certify that I have read this study and that in my opinion it conforms to acceptable standards of scholarly presentation and is fully adequate, in scope and quality, as a dissertation for the degree of Doctor of Philosophy.

Genevieve S. Roessler

Genevieve S. Roessler
Associate Professor of Nuclear Engineering Sciences

I certify that I have read this study and that in my opinion it conforms to acceptable standards of scholarly presentation and is fully adequate, in scope and quality, as a dissertation for the degree of Doctor of Philosophy.

Jeffrey R. Fitzsimmons
Associate Professor of Radiology

I certify that I have read this study and that in my opinion it conforms to acceptable standards of scholarly presentation and is fully adequate, in scope and quality, as a dissertation for the degree of Doctor of Philosophy.

Thomas H. Mareci

Thomas H. Mareci
Associate Professor of Physics

This dissertation was submitted to the Graduate Faculty of the College of Engineering and to the Graduate School and was accepted as partial fulfillment of the requirements for the degree of Doctor of Philosophy.

December 1989

Herbert A. Beaver
Dean, College of Engineering

Dean, Graduate School